



# CHORUS

This is the accepted manuscript made available via CHORUS. The article has been published as:

## Brownian thermal noise in multilayer coated mirrors

Ting Hong, Huan Yang, Eric K. Gustafson, Rana X. Adhikari, and Yanbei Chen

Phys. Rev. D **87**, 082001 — Published 2 April 2013

DOI: [10.1103/PhysRevD.87.082001](https://doi.org/10.1103/PhysRevD.87.082001)

# Brownian Thermal Noise in Multilayer Coated Mirrors

Ting Hong,<sup>1</sup> Huan Yang,<sup>1</sup> Eric K. Gustafson,<sup>2</sup> Rana X. Adhikari,<sup>2</sup> and Yanbei Chen<sup>1</sup>

<sup>1</sup>*Theoretical Astrophysics 350-17, California Institute of Technology, Pasadena, CA 91125, USA*

<sup>2</sup>*LIGO Laboratory 100-36, California Institute of Technology, Pasadena, CA 91125, USA*

We analyze the Brownian thermal noise of a multi-layer dielectric coating, used in high-precision optical measurements including interferometric gravitational-wave detectors. We assume the coating material to be isotropic, and therefore study thermal noises arising from shear and bulk losses of the coating materials. We show that coating noise arises not only from layer thickness fluctuations, but also from fluctuations of the interface between the coating and substrate, driven by fluctuating shear stresses of the coating. Although thickness fluctuations of different layers are statistically independent, there exists a finite coherence between the layers and the substrate-coating interface. In addition, photoelastic coefficients of the thin layers (so far not accurately measured) further influences the thermal noise, although at a relatively low level. Taking into account uncertainties in material parameters, we show that significant uncertainties still exist in estimating coating Brownian noise.

PACS numbers: 04.80.Nn, 05.40.+j

## I. INTRODUCTION

Brownian thermal noise in the dielectric coatings of mirrors limits some high precision experiments which use optical metrology. This thermal noise is currently a limit for fixed spacer Fabry-Perots used in optical clock experiments [1] and is estimated to be the dominant noise source in the most sensitive band of modern gravitational wave detectors (e.g., advanced LIGO, GEO, advanced VIRGO and KAGRA) [2–6]. Recent work has indicated the possibility of reducing the various kinds of internal thermal noise by redesigning the shape of the optical mode [7, 8] or the structure of the multi-layer coating [9, 10]. In this paper, we seek a more comprehensive understanding of coating Brownian noise. We first identify all thermally fluctuating physical properties (e.g., different components of the strain tensor) of the coating that can lead to Coating Brownian noise, and calculate how each of them contributes (linearly) to the total noise; we then calculate their individual levels of fluctuation, as well as cross correlations between pairs of them, using the Fluctuation Dissipation Theorem [11–13]. In this way, as we compute the total Coating Brownian noise, it will be clear how each factor contributes, and we will be in a better position to take advantage of possible correlations between different components of the noise.

As a starting point, we will assume each coating layer to be isotropic, and hence completely characterized by its complex bulk modulus  $K$  and shear modulus  $\mu$ —each with small imaginary parts related to the energy loss in the bulk and shear motions. The complex arguments of these moduli are often referred to as *loss angles*. While values of  $K$  and  $\mu$  are generally known, loss angles of thin optical layers vary significantly according to the details of the coating process (i.e., how coating materials are applied onto the substrate and their composition). Since the loss angles are small, we will use  $K$  and  $\mu$  to denote the real parts of the bulk and shear moduli, and write the complex bulk and shear moduli,  $\tilde{K}$  and  $\tilde{\mu}$  as

$$\tilde{K} = K(1 + i\phi_B), \quad \tilde{\mu} = \mu(1 + i\phi_S). \quad (1)$$

Here we have used subscripts  $B$  and  $S$  to denote bulk and shear, because these will be symbols for bulk strain and shear

strain.

Note that our definition differs from previous literature, which used  $\phi_{\parallel}$  and  $\phi_{\perp}$  to denote losses induced by elastic deformations parallel and perpendicular to the coating-substrate interface [14]. As we shall argue in Appendix III,  $\phi_{\parallel}$  and  $\phi_{\perp}$  cannot be consistently used as independent loss angles of a material. Only assuming  $\phi_{\parallel} = \phi_{\perp} = \phi_S = \phi_B$  will the previous calculation agree with ours — if we ignore light penetration into the coating. There is, a priori, no reason why these loss angles should all be equal, although this assumption has so far been compatible with existing ring-down measurements and direct measurements of coating thermal noise [15].

Brownian thermal fluctuations of a multilayer coating can be divided as follows: (i) thickness fluctuation of the coating layers, (ii) fluctuation of the coating-substrate interface, and (iii) refractive index fluctuations of the coating layers associated with longitudinal (thickness) and transverse (area) elastic deformations—as illustrated in Figure 1. Using what is sometimes referred to as Levin’s direct approach [12] (based on the fluctuation dissipation theorem) and writing the coating Brownian noise as a linear combination of the above fluctuations allows the construction of a corresponding set of forces acting on the coating and calculation of the thermal noise spectrum from the the dissipation associated with the simultaneous application of these forces. This has been carried out by Gurkovsky and Vyatchanin [16], as well as Kondratiev, Gorkovsky and Gorodetsky [17]. However, in order to obtain insights into coating noise that have proven useful we have chosen to calculate the cross spectral densities for each of (i), (ii), and (iii), and provide intuitive interpretations of each. We will show, in Sec. IV, that (i) and (ii) above are driven by both bulk and shear fluctuations in the coating, in such a way that thickness fluctuations of the  $j$ -th layer  $\delta l_j$ , or in transverse locations separated by more than a coating thickness, are mutually statistically independent, yet each  $\delta l_j$  is correlated with the fluctuation of the coating-substrate interface  $z_s$ —because  $z_s$  is driven by the *sum* of thermal stresses in the coating layers. We will also show that when coating thickness is much less than the beam spot size, the only significant contribution to (iii) arises from longitudinal (thickness) fluctuations, see

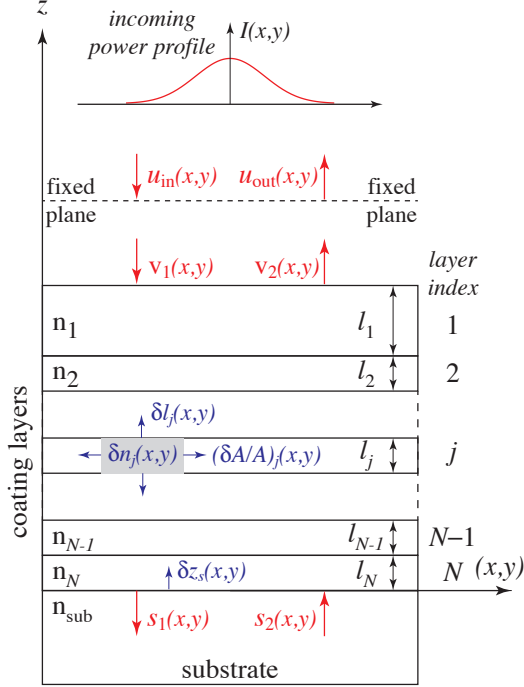


Figure 1: Drawing of a mirror coated with multiple dielectric layers. Shown here are the various fluctuations that contribute to coating noise, i.e., fluctuations in the amplitude and phase of the returning light caused by fluctuations in the geometry [including: layer thickness  $\delta l_j$ , layer area stretch  $(\delta A/A)_j$ , interface height  $z_s$  of the coating-substrate configuration] and in the refractive indices  $\delta n_j(x, y, z)$  of the layers.

Appendix ID for details.

This paper is organized as follows. In Sec. II, we express the amplitude and phase of the reflected field in terms of fluctuations in the coating structure, thereby identifying the various components of coating thermal noise. In Sec. III, we introduce the loss angles of isotropic coating materials, and use the Fluctuation-Dissipation Theorem to calculate the cross spectral densities of the coating thermal noise ignoring light penetration into the multi-layer coating. In Sec. IV, we discuss in detail the cross spectra of all the components of the coating structure fluctuation, thereby obtaining the full formula for coating thermal noise, taking light penetration within the multi-layers into account. The key formulas summarizing phase and amplitude noise spectrum is given in Eq. (94) and Eq. (95). In Sec. V, we discuss the effect of light penetration on coating thermal noise, using typical optical coating structures. In Sec. VI, we discuss the dependence of thermal noise on the material parameters, and optimize the coating structure in order to lower the thermal noise. In Sec. VII, we discuss how only one combination of the two loss angles have been measured in past experiments, and how other different combinations can be measured using a new experimental geometry. Finally, we summarize our main conclusions in Sec. VIII.

## II. COMPONENTS OF THE COATING THERMAL NOISE

In this section, we express the coating thermal noise in terms of the elastic deformations of the coated substrate.

### A. Complex Reflectivity

As illustrated in Figure 1, we consider a laser field normally incident (along the  $-z$  direction) onto the mirror, with complex amplitude profile  $u_{\text{in}}(x, y)$  at a fixed reference plane (dashed line in the figure) and intensity profile  $I(x, y) = |u_{\text{in}}(x, y)|^2$ . Henceforth in the paper, we shall use arrows (e.g.,  $\vec{x}$ ) to denote the 2-dimensional vector  $(x, y)$  in the *transverse plane*, and boldface letters (e.g.,  $\mathbf{x}$ ) to denote 3-dimensional vectors.

Because the coating thickness is much less than the beam spot size, the reflected field (traveling along the  $+z$  direction) at transverse location  $\vec{x}$  has an amplitude given by

$$u_{\text{out}}(\vec{x}) = \rho_{\text{tot}}(\vec{x}) u_{\text{in}}(\vec{x}), \quad (2)$$

which only depends on the complex reflectivity  $\rho_{\text{tot}}(\vec{x})$  and the complex amplitude of the incident field  $u_{\text{in}}(\vec{x})$ , at the same location  $\vec{x}$  — assuming no incident light from the substrate (i.e.,  $s_2 = 0$ ). Here  $\rho_{\text{tot}}(\vec{x})$  can be separated into three factors, as

$$\rho_{\text{tot}}(\vec{x}) = \frac{u_{\text{out}}(\vec{x})}{u_{\text{in}}(\vec{x})} = \left[ \frac{u_{\text{out}}(\vec{x})}{v_2(\vec{x})} \right] \left[ \frac{v_1(\vec{x})}{u_{\text{in}}(\vec{x})} \right] \left[ \frac{v_2(\vec{x})}{v_1(\vec{x})} \right] \quad (3)$$

in which  $v_1(\vec{x})$  is the incident complex amplitude at the coating-air interface, while  $v_2(\vec{x})$  is the reflected complex amplitude at that interface.

The first two phase factors on the right-hand side of Eq. (3) are gained by the light when traveling across the gap between the fixed reference plane (see Fig. 1) and the coating-air interface; we therefore obtain, up to a constant phase factor,

$$\left[ \frac{u_{\text{out}}(\vec{x})}{v_2(\vec{x})} \right] \left[ \frac{v_1(\vec{x})}{u_{\text{in}}(\vec{x})} \right] = e^{-2ik_0[\delta z_s(\vec{x}) + \sum_{j=1}^N \delta l_j(\vec{x})]} \quad (4)$$

where  $k_0 = \omega_0/c$  is the wave number of the laser ( $\omega_0$  its angular frequency) in vacuum,  $\delta z_s(\vec{x})$  is the vertical displacement of the coating-substrate interface (from its zero point), and  $\delta l_j(\vec{x})$  is the thickness fluctuation of the  $j$ -th coating layer — both evaluated at a transverse location  $\vec{x}$ .

The remaining complex reflectivity  $v_2(\vec{x})/v_1(\vec{x})$  can be determined as a function of the phase shift experienced by the field in each layer, as well as the reflectivity of each interface, as described in detail in Sec. V. We can write:

$$v_2/v_1 = \rho[\phi_1(\vec{x}), \dots, \phi_N(\vec{x}); r_{01}(\vec{x}), \dots, r_{Ns}(\vec{x})] \quad (5)$$

Here  $\rho$  is the complex reflectivity of a multi-layer coating, measured at the coating-air interface, which in turn depends on the optical thickness  $\phi_j(\vec{x})$  of each layer ( $j = 1, \dots, N$ ) and the reflectivity  $r_{p,p+1}(\vec{x}) \equiv r_p(\vec{x})$  of each interface, ( $p = 0, \dots, N$ , with  $p = N + 1$  representing the substrate, and  $p = 0$

the vacuum outside the coating). Assembling the above equations (3)–(5), we obtain:

$$\rho_{\text{tot}}(\vec{x}) = e^{-2ik_0[\delta z_s(\vec{x}) + \sum_{j=1}^N \delta l_j(\vec{x})]} \rho[\{\phi_j(\vec{x})\}; \{r_p(\vec{x})\}] \quad (6)$$

Brownian thermal forces lead to fluctuations in both the real and imaginary parts of this complex reflectivity. Fluctuations in the argument of the complex reflectivity phase modulates the out-going light and directly produces sensing noise. Fluctuations in the magnitude, on the other hand, amplitude modulate the out-going light, and produces a ponderomotive force noise.

## B. Thermal Phase and Amplitude Noise

Brownian thermal fluctuations in coating geometry and refractive index modify the complex reflectivity  $\rho_{\text{tot}}(\vec{x})$  defined in Eq. (6). The real and imaginary parts of

$$\delta \log \rho_{\text{tot}}(\vec{x}) = \frac{\delta \rho_{\text{tot}}(\vec{x})}{\rho_{\text{tot}}(\vec{x})} \quad (7)$$

encode the amplitude/intensity and phase fluctuations of the reflected light at position  $\vec{x}$  on the mirror surface. In particular, intensity fluctuation of the reflected light is given by

$$\frac{\delta I(\vec{x})}{I(\vec{x})} = 2 \frac{\delta |\rho_{\text{tot}}(\vec{x})|}{|\rho_{\text{tot}}(\vec{x})|} = 2 \text{Re} [\delta \log \rho_{\text{tot}}(\vec{x})] \quad (8)$$

while phase fluctuation is given by

$$\delta \phi(\vec{x}) = \delta \arg [\rho_{\text{tot}}(\vec{x})] = \text{Im} [\delta \log \rho_{\text{tot}}(\vec{x})] \quad (9)$$

In this way, if we further write

$$\xi(\vec{x}) - i\zeta(\vec{x}) = -\frac{i}{2k_0} \delta [\log \rho_{\text{tot}}], \quad (10)$$

with both  $\xi$  and  $\zeta$  real-valued functions of  $\vec{x}$ , with the dimensionality of displacement; they will represent phase and amplitude noise, respectively. In particular, from Eq. (9), we have

$$\delta \phi(\vec{x}) = 2k_0 \xi(\vec{x}), \quad (11)$$

Because we measure the mirror's position through the additional phase shift gained by the light after being reflected, through the relation  $\Delta\phi = 2k_0\Delta x$ , Eq. (11) indicates that  $\xi(\vec{x})$  is the displacement noise due to phase fluctuations of the reflected light imposed by the coating.

The quantity  $\zeta$  (which, like  $\xi$ , is a length) is connected to amplitude/intensity noise via

$$2k_0\zeta(\vec{x}) = \text{Re} [\delta \log \rho_{\text{tot}}] = \frac{\delta I(\vec{x})}{2I(\vec{x})}. \quad (12)$$

As we shall discuss in Sec. II E,  $\zeta$  will cause a fluctuating force on the mirror, and can eventually be converted to a displacement noise via a dimensionless factor, although the effect will turn out to be small for gravitational-wave detectors.

Inserting the dependence of  $\rho_{\text{tot}}$  on  $\rho$ ,  $l_j$  and  $z_s$  [Cf. Eq. (6)], we obtain

$$\begin{aligned} \xi(\vec{x}) - i\zeta(\vec{x}) &= -\delta z_s(\vec{x}) - \sum_{l=1}^N \delta l_l(\vec{x}) \\ &\quad - \sum_{j=1}^N \frac{i}{2k_0} \left[ \frac{\partial \log \rho}{\partial \phi_j} \cdot \delta \phi_j(\vec{x}) \right] \\ &\quad - \sum_{p=0}^N \frac{i}{2k_0} \left[ \frac{\partial \log \rho}{\partial r_p} \cdot \delta r_p(\vec{x}) \right]. \end{aligned} \quad (13)$$

The first two terms are due to the motion of the coating-air interface at location  $\vec{x}$  and thickness fluctuations of the layers, while the last two terms are due to light penetration into the coating layers (see Fig. 5). In particular, the third term is due to fluctuations in the total phase the light gains when propagating within the  $j$ -th layer, while the fourth term is due to the (effective) reflectivity of the  $p$ -th interface (with  $p = 0$  indicating the coating-air interface), whose origin will be explained below.

## C. Fluctuations $\delta\phi_j$ and $\delta r_p$

Light propagating within the coating layers are affected by the *photoelastic* effect, namely an *isothermal* fluctuation in  $\delta n_j(\mathbf{x})$  (note here that  $\mathbf{x}$  is a 3-D vector) due to fluctuating Brownian stresses exerted onto the coating materials. Assuming *isotropy* of the coating materials, we can write

$$\delta n_j(\mathbf{x}) = \beta_j^L S_{zz}(\mathbf{x}) + \beta_j^T [S_{xx}(\mathbf{x}) + S_{yy}(\mathbf{x})] \quad (14)$$

with

$$\beta_j^L \equiv \left( \frac{\partial n_j}{\partial \log l} \right)_{A_j}, \quad \beta_j^T \equiv \left( \frac{\partial n_j}{\partial \log A} \right)_{l_j} \quad (15)$$

Here  $L$  stands for longitudinal, and  $T$  stands for transverse, and the subscript  $A_j$  and  $l_j$  indicate fixing transverse area and longitudinal length, respectively. We have also used the usual strain definition

$$S_{ij} \equiv \frac{1}{2} \left[ \frac{\partial u_i}{\partial x_j} + \frac{\partial u_j}{\partial x_i} \right] \quad (16)$$

where  $u_i(\mathbf{x})$ ,  $i = 1, 2, 3$  are components of the displacement vector of the mass element at position  $\mathbf{x}$ . Refer to Appendix II for more details in defining the elasticity quantities, and Appendix A 1 for more details on the photo elastic effect.

We note that in Eq. (14)  $S_{zz}$  is the fractional increase in length (i.e., linear expansion) in the longitudinal direction, while  $S_{xx} + S_{yy}$  is the fractional increase in the transverse area. According to Appendix ID, we can ignore the second term representing area fluctuations in Eq. (14) when the beam spot size is much larger than the coating thickness. In this case, we write  $\beta_j$  in place for  $\beta_j^L$ , whose value can be expressed in terms of a particular component of the photo elastic tensor, see Eq. (A5).

As we discuss in Appendix A 2, the first term of Eq. (14) causes two effects for light propagating along each direction (i.e.,  $+z$  and  $-z$ ): it adds an additional phase shift, and it back-scatters a fraction of the light into the opposite direction. As we show in Appendix IC [c.f. Eqs. (16)–(18)], these effects can be accounted for by modifying the phase shift  $\delta\phi_j$  of each coating layer and changing the reflectivity  $\delta r_j$  of interface, in the following manner:

$$\delta\phi_j = k_0 \left[ (n_j + \beta_j) \delta l_j - \frac{1 - r_j^2}{2r_j} \beta_j \delta l_j^c + \frac{1 + r_{j-1}^2}{2r_{j-1}} \beta_{j-1} \delta l_{j-1}^c \right], \quad (17)$$

$$\delta r_j = k_0 t_j^2 \beta_j \delta l_j^s. \quad (18)$$

Here we have defined

$$\delta l_j^c = - \int_0^{l_j} S_{zz}(z_{j+1} + z) \cos(2k_0 n_j z) dz \quad (19)$$

$$\delta l_j^s = - \int_0^{l_j} S_{zz}(z_{j+1} + z) \sin(2k_0 n_j z) dz \quad (20)$$

for  $j \geq 1$ ,  $\delta l_0^s = \delta l_0^c = 0$ , and

$$z_j \equiv \sum_{n=j}^N l_n. \quad (21)$$

marks the  $z$ -coordinate of the top surface of the  $j$ -th layer. We can also write

$$\delta l_j = \int_0^{l_j} S_{zz}(z_{j+1} + z) dz. \quad (22)$$

Note that

$$\text{total coating thickness} \equiv z_1 > z_2 > \dots > z_{N+1} \equiv 0 \quad (23)$$

Note that  $\delta r_j$ , as well as the last two terms in  $\delta\phi_j$  are due to back-scattering, and have not been considered by previous authors.

Inserting Eqs. (17), (18) into Eq. (13), we obtain:

$$\xi(\vec{x}) - i\zeta(\vec{x}) = -z_s(\vec{x}) - \sum_{j=1}^N \int_{z_{j+1}}^{z_j} \left[ 1 + \frac{i\epsilon_j(z)}{2} \right] u_{zz}(\vec{x}, z) dz \quad (24)$$

where

$$\begin{aligned} \epsilon_j(z) = & (n_j + \beta_j) \frac{\partial \log \rho}{\partial \phi_j} \\ & - \beta_j \left[ \frac{1 - r_j^2}{2r_j} \frac{\partial \log \rho}{\partial \phi_j} \right. \\ & \quad \left. - \frac{1 + r_j^2}{2r_j} \frac{\partial \log \rho}{\partial \phi_{j+1}} \right] \cos[2k_0 n_j (z - z_j)] \\ & - t_j^2 \beta_j \frac{\partial \log \rho}{\partial r_j} \sin[2k_0 n_j (z - z_{j+1})], \end{aligned} \quad (25)$$

a term that accounts for all effects associated with light penetration. Here we need to formally define

$$\frac{\partial \log \rho}{\partial \phi_{N+1}} = 0 \quad (26)$$

because  $\phi_{N+1}$  does not really exist. Alternatively, we can also write formulas separately for  $\xi$  and  $\zeta$ , using only real-valued quantities. For  $\xi$ , we have,

$$\begin{aligned} \xi(\vec{x}) = & -z_s(\vec{x}) \\ & - \sum_{j=1}^N \left[ \mathcal{T}_j^\xi \delta l_j(\vec{x}) + \mathcal{T}_j^{\xi c} \delta l_j^c(\vec{x}) + \mathcal{T}_j^{\xi s} \delta l_j^s(\vec{x}) \right], \end{aligned} \quad (27)$$

where

$$\mathcal{T}_j^\xi = 1 - \frac{n_j + \beta_j}{2} \text{Im} \left( \frac{\partial \log \rho}{\partial \phi_j} \right) \quad (28)$$

$$\begin{aligned} \mathcal{T}_j^{\xi c} = & -\frac{\beta_j}{4} \text{Im} \left( \frac{\partial \log \rho}{\partial \phi_j} \right) \left( \frac{1 - r_j^2}{r_j} \right) \\ & + \frac{\beta_j}{4} \text{Im} \left( \frac{\partial \log \rho}{\partial \phi_{j+1}} \right) \left( \frac{1 + r_j^2}{r_j} \right) \end{aligned} \quad (29)$$

$$\mathcal{T}_j^{\xi s} = -\frac{\beta_j t_j^2}{2} \text{Im} \left( \frac{\partial \log \rho}{\partial r_j} \right) \quad (30)$$

are transfer functions from the various  $\delta l$ 's to the displacement-equivalent thermal noise (see Fig. 6). For  $\zeta$ , we have

$$\zeta(\vec{x}) = \sum_{j=1}^N \left[ \mathcal{T}_j^\zeta \delta l_j(\vec{x}) + \mathcal{T}_j^{\zeta c} \delta l_j^c(\vec{x}) + \mathcal{T}_j^{\zeta s} \delta l_j^s(\vec{x}) \right] \quad (31)$$

where

$$\mathcal{T}_j^\zeta = \frac{n_j + \beta_j}{2} \text{Re} \left( \frac{\partial \log \rho}{\partial \phi_j} \right) \quad (32)$$

$$\begin{aligned} \mathcal{T}_j^{\zeta c} = & \frac{\beta_j}{4} \text{Re} \left( \frac{\partial \log \rho}{\partial \phi_j} \right) \left( \frac{1 - r_j^2}{r_j} \right) \\ & - \frac{\beta_j}{4} \text{Re} \left( \frac{\partial \log \rho}{\partial \phi_{j+1}} \right) \left( \frac{1 + r_j^2}{r_j} \right) \end{aligned} \quad (33)$$

$$\mathcal{T}_j^{\zeta s} = \frac{\beta_j t_j^2}{2} \text{Re} \left( \frac{\partial \log \rho}{\partial r_j} \right) \quad (34)$$

For an arbitrary stack of dielectrics,  $\zeta$  is comparable to the part of  $\xi$  [c.f. Eq. (25)] that involves light penetration into the layers. In practice, however, for highly reflective stacks, the real parts of  $\partial \log \rho / \partial \phi_j$  and  $\partial \log \rho / \partial r_j$  all turn out to be small, and therefore fluctuations in  $\zeta$  (which corresponds to amplitude fluctuations) should be much less than fluctuations in  $\xi$  (which corresponds to phase fluctuations).

#### D. Mode selection for phase noise

So far we have dealt with phase and amplitude noise as functions at each location  $\vec{x}$  on the mirror surface. However,

there is only one displacement noise that the light will sense. In this and the next subsection, we show how  $\xi(\vec{x})$  and  $\zeta(\vec{x})$  should be converted into measurement noise. In doing so, we recognize that only one spatial optical mode is injected on resonance in the optical cavity, and this mode has a complex amplitude of  $u_0(\vec{x})$  at the mirror surface. Now suppose we have  $u_{\text{in}} = u_0(\vec{x})$  incident on the mirror surface, we will then have  $u_{\text{out}}(\vec{x}) = \rho_{\text{tot}}(\vec{x})u_0(\vec{x})$ , which contains not only the resonant mode, but also other modes, which do not resonate in the cavity.

Let us select only the component of  $u_{\text{out}}(\vec{x})$  that is in the resonant spatial mode that is driven, then we have a complex reflectivity of

$$\bar{\rho} = \frac{\int u_0^*(\vec{x})u_{\text{out}}(\vec{x})d^2\vec{x}}{\int u_0^*u_0d^2\vec{x}} = \frac{\int \rho_{\text{tot}}(\vec{x})I(\vec{x})d^2\vec{x}}{\int I(\vec{x})d^2\vec{x}}, \quad (35)$$

specifically for the resonant mode, and hence independent of  $\vec{x}$ . Here we have defined  $I(\vec{x}) \equiv |u_0(\vec{x})|^2$ . Note that the bar on top of  $\bar{\rho}$  represents averaging over the phase front, instead of averaging over time.

Now, inserting Eq. (10) as definitions for  $\xi(\vec{x})$  and  $\zeta(\vec{x})$  into Eq. (35), we obtain the fluctuating part of  $\bar{\rho}$

$$\frac{\delta\bar{\rho}}{\bar{\rho}} = 2ik_0(\bar{\xi} - i\bar{\zeta}), \quad (36)$$

where

$$\bar{\xi} \equiv \frac{\int \xi(\vec{x})I(\vec{x})d^2\vec{x}}{\int I(\vec{x})d^2\vec{x}}, \quad \bar{\zeta} \equiv \frac{\int \zeta(\vec{x})I(\vec{x})d^2\vec{x}}{\int I(\vec{x})d^2\vec{x}}. \quad (37)$$

Note that  $2ik_0\bar{\xi}$  is the additional phase gained by the returning light, while  $2k_0\bar{\zeta}$  is the relative change in amplitude [see discussions in Sec. II B]. Focusing first on  $\bar{\xi}$ , we note that this creates the same phase change as that gained by the reflected light if the mirror does not deform but instead is displaced along the beam by  $\bar{\xi}$ . In this way,  $\bar{\xi}$  is an error in our measurement of the mirror's displacement.

### E. Conversion of Amplitude Noise into Displacement

The amplitude thermal noise can produce a spurious GW signal by modulating the radiation pressure acting on the mirror, which in turn drives spurious mirror motion. Let us first consider a single-bounce scenario, in which an incoming beam with intensity profile  $I(\vec{x})$ , unaffected by thermal noise, is reflected with an intensity profile  $I(\vec{x}) + \delta I(\vec{x})$ , with  $\delta I(\vec{x})$  induced by amplitude thermal noise. In this case, the mirror feels a thermal-noise-induced recoil force of

$$F_{\text{th}}^{\text{single}} = \int \frac{\delta I(\vec{x})}{c} d^2\vec{x}. \quad (38)$$

Using Eqs. (12) and (37), we obtain

$$F_{\text{th}}^{\text{single}} = \frac{4I_0k_0}{c}\bar{\zeta} \quad (39)$$

with  $I_0$  the power incident on the mirror. If the mirror is within a cavity, then we need to consider both the increase in the circulating power (which we denote by  $I_c$ ) with respect to the input power, and the coherent build-up of amplitude modulation within the cavity. We also note that now both the incident and reflected beam contains amplitude modulation, and that we must also consider the effect of this amplitude modulation on the input mirror.

If we restrict ourselves to a single optical cavity on resonance, then the force thermal noise below the cavity bandwidth is given by

$$F_{\text{th}}^{\text{cav}} = \frac{16k_0I_c}{c\sqrt{T_i}}\bar{\zeta} \quad (40)$$

Here  $I_c$  is the circulating power in the arm cavity. Suppose both input and end mirrors have the same mass  $M$ , then the spectrum of cavity length modulation driven by the amplitude thermal noise at angular frequency  $\Omega$  is given by

$$\sqrt{S_{\text{th}}^{\text{amp}}(\Omega)} = \frac{2}{M\Omega^2}\sqrt{S_{F_{\text{th}}^{\text{cav}}}} = \frac{32\omega_0I_c}{m\Omega^2c^2\sqrt{T_i}}\sqrt{S_{\bar{\zeta}}} \quad (41)$$

Note that  $\bar{\zeta}$  has the units of displacement, and therefore the pre-factor in front of  $\sqrt{S_{\bar{\zeta}}}$  in Eq. (41) is a dimensionless conversion factor from  $\bar{\zeta}$  to displacement noise. For Advanced LIGO, this cannot be completely dismissed at this stage, because

$$\frac{32\omega_0I_c}{m\Omega^2c^2\sqrt{T_i}} = 18 \cdot \frac{I_c}{800\text{ kW}} \cdot \frac{40\text{ kg}}{m} \cdot \left[\frac{10\text{ Hz}}{\Omega/(2\pi)}\right]^2 \sqrt{\frac{0.03}{T_i}} \quad (42)$$

Nevertheless, as we will show in Sec. V B, the minor amplification factor here is not enough to make amplitude noise significant, because  $\zeta$  is much less than  $\xi$ , for the coatings we consider.

## III. THERMAL NOISE ASSUMING NO LIGHT PENETRATION INTO THE COATING

In this section, we compute the coating Brownian noise assuming that the incident light does not penetrate into the coating. This means light is promptly reflected at the coating-air interface, and therefore we should only keep the first two terms on the right-hand side of Eq. (13), which leads to  $\zeta = 0$ . We therefore consider only coating phase noise  $\xi$ , in particular its weighted average over the mirror surface,  $\bar{\xi}$ , see Eq. (37).

### A. The Fluctuation-Dissipation Theorem

The Fluctuation-Dissipation Theorem relates the near-equilibrium thermal noise spectrum of a generalized coordinate  $q$  to the rate of dissipation in the system when a generalized force acts directly on this coordinate. More specifically, the thermal noise spectrum of  $q$  at temperature  $T$  is given by [13]

$$S_q(f) = \frac{k_B T}{\pi^2 f^2} \text{Re}[Z(f)] \quad (43)$$

where  $f$  is frequency,  $Z(f)$  is the mechanical impedance (inverse of admittance), or

$$Z(f) = -2\pi i f q(f) / F(f) \quad (44)$$

Alternatively, suppose we apply a sinusoidal force

$$F(t) = F_0 \cos(2\pi f t) \quad (45)$$

with amplitude  $F_0$  acting directly on  $q$ , Eq. (43) can also be written as

$$S_x(f) = \frac{4k_B T}{\pi f} \frac{W_{\text{diss}}}{F_0^2} = \frac{4k_B T}{\pi f} \frac{U}{F_0^2} \phi \quad (46)$$

where  $W_{\text{diss}}$  is the energy dissipated per cycle of oscillation divided by  $2\pi$  (in other words,  $W_{\text{diss}}$  is the average energy loss per radian),  $U$  is the peak of the stored energy in the system, and  $\phi$  is the loss angle, defined by

$$\phi = \text{Re}[Z(f)] / \text{Im}[Z(f)] \quad (47)$$

It is important to note that  $\phi$  is in general frequency dependent. However, for an elastic body, if the frequency is low enough (well below the first eigenfrequency), then  $U$  can be computed using the quasi-static approximation, because it is equal to the elastic energy stored in the equilibrium configuration when a constant force  $F_0$  is applied to the system.

## B. Mechanical Energy Dissipations in Elastic Media

It is straightforward to apply Eq. (46) to calculate the thermal noise component due to fluctuation of the position of the coating-air interface — the weighted average [c.f. Eq. (35)] of the first two terms of Eq. (13). This can be obtained by applying a force  $F$  with a pressure profile proportional to  $I(\vec{x})$  to the mirror surface (coating-air interface). In this case, elastic energy can be divided into bulk energy  $U_B$  and shear energy  $U_S$  [Chapter I of Ref. [18]], with

$$U_{\text{coating}} = U_B + U_S = \int_{\text{coating}} \left( \frac{K}{2} \Theta^2 + \mu \Sigma_{ij} \Sigma_{ij} \right) dV, \quad (48)$$

where  $\Theta$  is the expansion, and  $\Sigma_{ij}$  is the shear tensor (see Appendix II for details). If we give small imaginary parts to  $K$  and  $\mu$ , writing

$$\tilde{K} = K(1 + i\phi_B), \quad \tilde{\mu} = \mu(1 + i\phi_S) \quad (49)$$

then  $W_{\text{diss}}$  can be written as

$$W_{\text{diss}} = \phi_B U_B + \phi_S U_S \quad (50)$$

Here we have introduced the loss angles  $\phi_B$  and  $\phi_S$ , which are associated with the dissipation of expansion energy density and the shear energy density, respectively. Note that our way of characterizing loss differs from previous work by Harry, et. al. [14], because for isotropic materials,  $\phi_B$  and  $\phi_S$  are the two fundamentally independent loss angles that characterize the dissipation of bulk and shear elastic energy; were we to

literally adopt  $\phi_{\perp}$  and  $\phi_{\parallel}$  as done in Ref. [14], and consider them independent from each other, then the dissipated energy defined this way can turn out to be negative if certain force distribution are applied onto the mirror, which would be unphysical. See Appendix III for more details.

Once we have introduced  $\phi_B$  and  $\phi_S$ , other elastic moduli also gain small imaginary parts correspondingly. For example, for the most widely used Young's modulus and Poisson ratio, because

$$K = \frac{Y}{3(1-2\sigma)}, \quad \mu = \frac{Y}{2(1+\sigma)} \quad (51)$$

we can write

$$\tilde{Y} = Y(1 + i\phi_Y) \quad (52)$$

with

$$\phi_Y = \frac{(1-2\sigma)\phi_B + 2(1+\sigma)\phi_S}{3} \quad (53)$$

and

$$\tilde{\sigma} = \sigma + \frac{i}{3}(1-2\sigma)(1+\sigma)(\phi_B - \phi_S). \quad (54)$$

Since  $-1 < \sigma < 1/2$ , we have  $(1-2\sigma)(1+\sigma) > 0$ , therefore  $\tilde{\sigma}$  has a positive imaginary part as  $\phi_B$  is greater than  $\phi_S$ , and vice versa. To understand the physical meaning of the imaginary part of Poisson ratio, one has to realize that Young's modulus and Poisson ratio together describe the elastic response of a rod. Suppose we apply an oscillatory tension uniformly along a rod at a very low frequency, whether the area of the rod leads or lags the length of the rod depends on the relative magnitudes of the bulk and shear loss angles. In the situation when the two loss angles  $\phi_B$  and  $\phi_S$  are equal to each other, the Poisson's ratio is real, and we only need to deal with one loss angle  $\phi_Y$  — although there is reason to assume the equality of these two angles.

If the coating material is made into the shape of a one-dimensional rod, and if we only consider its elongational, bending or torsional modes, then the Young's modulus is the appropriate elastic modulus associated with these modes, and  $\phi_Y$  is the appropriate loss angle to apply. However, this is not directly relevant for coating thermal noise. An elastic modulus that will actually prove useful is that of the *two-dimensional (2-D) flexural rigidity* of a thin plate made from the coating material,

$$D = \frac{Yh}{12(1-\sigma^2)} = |D|(1 + i\phi_D) \quad (55)$$

where  $h$  is the thickness of the plate, with

$$\phi_D = \frac{(1-\sigma-2\sigma^2)\phi_B + 2(1-\sigma+\sigma^2)\phi_S}{3(1-\sigma)}. \quad (56)$$

As we shall see in Sec. VII A, this  $D$  is most easily measured through the quality factor of drum modes of a thinly coated sample — although this will not turn out to be the combination of loss angles that appear in the thermal noise of coated mirrors.

### C. Thermal Noise of a Mirror Coated with one Thin Layer

In the case where the coating thickness is much less than the size of the mirror substrate and the beam spot size, the elastic deformation of the substrate is not affected by the presence of the coating. As a consequence, if we include the elastic energy stored in the substrate  $U_{\text{sub}}$  with loss angle  $\phi_{\text{sub}}$ , we can write

$$\begin{aligned} W_{\text{diss}} &= \phi_{\text{sub}} U_{\text{sub}} + \phi_B U_B + \phi_S U_S \\ &\approx \left[ \phi_{\text{sub}} + \phi_B \frac{U_B}{U_{\text{sub}}} + \phi_S \frac{U_S}{U_{\text{sub}}} \right] U_{\text{sub}} \end{aligned} \quad (57)$$

With the assumption of thin coating and half-infinite substrate, the total strain energy stored in the sample can be considered as  $U_{\text{sub}}$ . In such a way the coating adds on to substrate loss angle as additional, effective angles

$$\phi_{\text{coated}} = \phi_{\text{sub}} + \frac{U_B}{U_{\text{sub}}} \phi_B + \frac{U_S}{U_{\text{sub}}} \phi_S \quad (58)$$

Note that when the total coating thickness  $l$  is much less than the beam spot size  $w_0$ , we have  $U_B/U_{\text{sub}} \sim U_S/U_{\text{sub}} \sim l/w_0 \ll 1$ . Unfortunately, however,  $\phi_B$  and  $\phi_S$  are found to be so much larger than the substrate loss angle  $\phi_{\text{sub}}$  that in practice coating thermal noise still dominates over substrate thermal noise.

Now suppose we would like to measure a weighted average of the position of the mirror surface,

$$q = \bar{\xi} = \int d^2 \vec{x} w(\vec{x}) z(\vec{x}) \quad (59)$$

with [Cf. Eq. (37)]

$$w(\vec{x}) = \frac{I(\vec{x})}{\int I(\vec{x}) d^2 \vec{x}} \quad (60)$$

and  $z(\vec{x})$  the position of the coating-air interface at transverse location  $\vec{x}$ .

According to Sec. III A, we need to apply a pressure profile of

$$f(\vec{x}) = F_0 w(\vec{x}) \quad (61)$$

onto the upper surface of the coating, which we shall also refer to as the coating-air interface. Straightforward calculations give

$$\begin{aligned} \frac{U_B}{F_0^2} &= \frac{(1-2\sigma_c)l}{3} \left[ \frac{Y_c}{Y_s^2} \frac{(1-2\sigma_s)^2(1+\sigma_s)^2}{(1-\sigma_c)^2} \right. \\ &\quad + \frac{1}{Y_s} \frac{2(1-2\sigma_s)(1+\sigma_s)(1+\sigma_c)}{(1-\sigma_c)^2} \\ &\quad \left. + \frac{1}{Y_c} \frac{(1+\sigma_c)^2}{(1-\sigma_c)^2} \right] \int w^2(\vec{x}) d^2 \vec{x} \end{aligned} \quad (62)$$

$$\begin{aligned} \frac{U_S}{F_0^2} &= \frac{2l}{3} \left[ \frac{Y_c}{Y_s^2} \frac{(1-\sigma_c + \sigma_c^2)(1+\sigma_s)^2(1-2\sigma_s)^2}{(1-\sigma_c)^2(1+\sigma_c)} \right. \\ &\quad - \frac{(1+\sigma_c)(1-2\sigma_c)(1-2\sigma_s)(1+\sigma_s)}{Y_s(1-\sigma_c)^2} \\ &\quad \left. + \frac{(1-2\sigma_c)^2(1+\sigma_c)}{Y_c(1-\sigma_c)^2} \right] \int w^2(\vec{x}) d^2 \vec{x} \end{aligned} \quad (63)$$

Here  $l$  is coating thickness; for Young's modulus  $Y$  and Poisson's ratio  $\sigma$ , substrates  $c$  and  $s$  represent coating and substrate, respectively. Directly following Eqs. (46) and (50) will give rise to a noise spectrum of

$$S_{\bar{\xi}} = \frac{4k_B T}{\pi f} \left[ \phi_B \frac{U_B}{F_0^2} + \phi_S \frac{U_S}{F_0^2} \right] \quad (64)$$

where  $U_B/F_0^2$  and  $U_S/F_0^2$  are given by Eqs. (62) and (63) respectively.

Here we can define

$$\int w^2(\vec{x}) d^2 \vec{x} = \frac{\int d^2 \vec{x} I^2(\vec{x})}{\left[ \int d^2 \vec{x} I(\vec{x}) \right]^2} \equiv \frac{1}{\mathcal{A}_{\text{eff}}} \quad (65)$$

as the inverse of an *effective beam area*. Therefore noise power in  $q$  is proportional to coating thickness and inversely proportional to beam area. In particular, for a Gaussian beam with

$$I(\vec{x}) \propto \exp\left(-\frac{2x^2}{w_0^2}\right) \quad (66)$$

the effective area is  $\mathcal{A}_{\text{eff}} = \pi w_0^2$ .

Let us compare our results to previous calculations using  $\phi_{\perp}$  and  $\phi_{\parallel}$ . As it turns out, if we assume  $\phi_S = \phi_B$ , then formulas for thermal noise agree with Eq. (22) in Ref. [14]. To illustrate the different roles now played by  $\phi_B$  and  $\phi_S$ , let us take the very simple case of  $Y = Y_c = Y_s$  and  $\sigma = \sigma_c = \sigma_s$ , where

$$\frac{\delta U_B}{F_0^2} = \frac{4l}{3Y\mathcal{A}_{\text{eff}}} (1+\sigma)^2 (1-2\sigma) \quad (67)$$

$$\frac{\delta U_S}{F_0^2} = \frac{2l}{3Y\mathcal{A}_{\text{eff}}} (1+\sigma)(1-2\sigma)^2 \quad (68)$$

Using Eq. (64), we can get the power spectral density of the single layer non-penetration coating thermal noise as

$$\begin{aligned} S_{\bar{\xi}}(f) &= \frac{8k_B T (1-\sigma-2\sigma^2)l}{3\pi f Y \mathcal{A}_{\text{eff}}} [2(1+\sigma)\phi_B + (1-2\sigma)\phi_S]. \end{aligned} \quad (69)$$

From Eq. (69), we can see that the bulk loss and shear loss contribute differently to the total noise. More importantly, at least in the simple case where  $Y_c = Y_s$ , the combination of  $\phi_B$  and  $\phi_S$ , is approximately  $2\phi_B + \phi_S$ , which differs significantly from the combination  $\phi_{\text{tot}} \approx \phi_B + 2\phi_S$  measured by the ring-down experiments that have been performed so far [19–21]. This will be discussed in detail in the rest of Sec. VII.

### D. Discussions on the correlation structure of thermal noise

Before proceeding to more detailed calculations of Brownian noise that involve light penetrating into the coating layers, we would like to gain more insight about thermal noise by



inspecting our existing expressions of coating thermal noise [Eqs. (62)–(64)] more carefully. We note that

$$S_{\tilde{\xi}} \propto l \int w^2(\vec{x}) d^2\vec{x}. \quad (70)$$

where the coefficient of proportionality depends only on material property. From such a dependence on coating and beam geometries, we deduce that (i) each point on the coating-air interface fluctuates along the  $z$  direction independently, and (ii) materials at different  $z$ 's within the coating also contribute independently to coating thermal noise. These observations will be confirmed below in Sec. IV.

Finally, within the coefficient of proportionality [Cf. Eqs. (62) and (63)], we found three types of dependence on the Young's moduli of the coating and substrate materials: terms proportional to  $1/Y_c$  are expected to arise from fluctuations in coating thickness, terms proportional to  $Y_c/Y_s^2$  can be interpreted as arising from coating thermal stresses driving the substrate-coating interface, while terms proportional to  $1/Y_s$  are therefore interpreted as correlations between the above two types of noise.

#### IV. CROSS SPECTRA OF THERMAL NOISE COMPONENTS

In this section, we compute the cross spectra of each component of coating thermal noise, and assemble the formula for the spectral density of the total noise. Specifically, in Sec. IV A, we compute the cross spectra of the thickness fluctuations between any two uniform sublayers of the coating, and obtain the cross spectrum of  $S_{zz}$ ; in Sec. IV B, we compute the cross spectra involving height fluctuation  $z_s$  of the coating-substrate interface, i.e.,  $S_{S_{zz}z_s}$  and  $S_{z_s z_s}$ ; in Sec. IV C, we dissect the above results and analyze the separate roles of bulk and shear fluctuations; in Sec. IV D, we write down the full formula for coating thermal noise.

##### A. Coating-Thickness Fluctuations

Let us start by calculating thickness fluctuations of individual layers and correlations between them. Following Levin's approach, we imagine applying two pairs of opposite pressure,

$$f_1(\vec{x}) = F_0 w_1(\vec{x}), \quad f_3(\vec{x}) = F_0 w_3(\vec{x}) \quad (71)$$

in the  $z$  direction on layer I and layer III, as shown in Fig. 2, with thickness of  $l_1$  and  $l_3$ , respectively. Here  $w_1(\vec{x})$  and  $w_3(\vec{x})$ , like the  $w(\vec{x})$  used in Eq. (59), provides the shape of the pressure profiles. Note that we apply pairs of forces, and each pair must be equal and opposite in direction because we are interested in learning about the fluctuations of the *thickness*, instead of the location, of the layers.

We assume that layers I and III are each made from a single type of material, yet there could be arbitrary number of different material sub layers in II. As it will turn out, the precise locations of layers I and III along the  $z$  direction does not

affect the result, *as long as they do not overlap*, or in other words, layer II has non-zero thickness.

Throughout this paper, we shall assume that the beam spot size is much less than the radius of the mirror, so that we can make the approximation that the mirror surface is an infinite two-dimensional plane. In this case, we perform a spatial Fourier transformation for the applied pressure,

$$\tilde{f}_j(\vec{k}) = \int e^{i\vec{k}\cdot\vec{x}} f_j(\vec{x}) d^2\vec{x} = F_0 \tilde{w}_j(\vec{k}), \quad j = 1, 3, \quad (72)$$

and carry out our calculations for strain and stress distributions in the coating-substrate system in the Fourier domain.

We further assume that the coating thickness is much less than the beam spot size, which is inverse the maximum spatial frequency contained in  $\tilde{w}_{1,3}$ . This means we only need to consider  $\vec{k}$ 's with  $|\vec{k}|l \ll 1$ , with  $l$  the total coating thickness. According to calculations in Appendix II, non-zero components of the stress and strain tensors in Layers I and III are found to be (in the spatial Fourier domain)

$$\tilde{T}_{xx}^I = \tilde{T}_{yy}^I = \frac{\sigma_1 \tilde{w}_1}{1 - \sigma_1} F_0, \quad \tilde{T}_{zz}^I = \tilde{w}_1 F_0, \quad (73)$$

$$\tilde{S}_{zz}^I = -\frac{(1 - 2\sigma_1)(1 + \sigma_1)\tilde{w}_1}{Y_1(1 - \sigma_1)} F_0, \quad (74)$$

and

$$\tilde{T}_{xx}^{III} = \tilde{T}_{yy}^{III} = \frac{\sigma_3 \tilde{w}_3}{1 - \sigma_3} F_0, \quad \tilde{T}_{zz}^{III} = \tilde{w}_3 F_0, \quad (75)$$

$$\tilde{S}_{zz}^{III} = -\frac{(1 - 2\sigma_3)(1 + \sigma_3)\tilde{w}_3}{Y_3(1 - \sigma_3)} F_0, \quad (76)$$

respectively.

Note that deformations within layer I only depends on  $\tilde{w}_1$  (not  $\tilde{w}_3$ ), while deformations within layer III only depends on  $\tilde{w}_3$  (not  $\tilde{w}_1$ ) — while regions outside these layers are found to have vanishing strain and stress. This means we can treat deformations caused by each pair of forces independently, as long as layer I and layer III do not overlap. The deformations are also independent of the thickness of the layers. The vanishing of deformations outside these layers means that when we introduce additional pairs of opposite forces, the new deformations introduced will be constrained within those new layers — as long as those new layers do not overlap with existing ones. This independence originates from the linearity of elastic response, and the fact that coating strains induced by force applied on a single surface within the coating, as discussed in Appendix II, do not depend on distance away from that surface, as seen in Eqs. (25)–(32). The situation here is analogous to the electrostatics of several pairs of oppositely-charged infinite parallel planes.

In terms of thermal noise, such a distribution of elastic deformations corresponds to a dissipation energy that consists of two independent terms, each corresponding to one layer and proportional to its thickness:

$$\frac{W_{\text{diss}}}{F_0^2} = W_{11} l_1 \int w_1^2 d^2\vec{x} + W_{33} l_3 \int w_3^2 d^2\vec{x} \quad (77)$$

Here we have defined, for  $j = 1, 3$ :

$$W_{jj} \equiv \frac{(1 - 2\sigma_j)(1 + \sigma_j)}{3(1 - \sigma_j)^2 Y_j} \left[ \frac{1 + \sigma_j}{2} \phi_B^j + (1 - 2\sigma_j) \phi_S^j \right]. \quad (78)$$

This means the fluctuation of

$$q \equiv \int [w_1(\vec{x})\delta l_1(\vec{x}) + w_3(\vec{x})\delta l_3(\vec{x})] d^2 \vec{x} \quad (79)$$

is given by

$$S_q = \frac{4k_B T}{\pi f} \sum_{j=1,3} \left[ W_{jj} l_j \int w_j^2(\vec{x}) d^2 \vec{x} \right] \quad (80)$$

The absence of a cross term between  $w_1$  and  $w_3$  means that fluctuations in  $\delta l_1(\vec{x})$  and  $\delta l_3(\vec{x})$  are uncorrelated — and hence statistically independent. Furthermore, within each layer, in the same spirit as the discussions in Sec. III D, the particular form of dependence on  $l_j$  and  $w_j(\vec{x})$  indicates that  $S_{zz}$  fluctuations at different 3-D locations (within this layer) are all uncorrelated and have the same spectrum. In this way, we obtain the cross spectral density of  $S_{zz}$  at two arbitrary 3-D locations within the coating:

$$S_{S_{zz}}^{ij}(\vec{x}, z; \vec{x}', z') = \frac{4k_B T}{\pi f} \delta_{ij} \delta^{(2)}(\vec{x} - \vec{x}') \delta(z - z') W_{jj} \quad (81)$$

Here we have assumed that  $(\vec{x}, z)$  belongs to layer  $i$ , while  $(\vec{x}', z')$  belongs to layer  $j$ . (The association to layers helps to identify the material property to be used in  $W_{jj}$ .)

## B. Fluctuations of Coating-Substrate Interface and their correlations with coating thickness

To investigate the correlation between the height of the coating-substrate interface,  $z_s(\vec{x})$  and the thickness of each coating layer,  $\delta l_j(\vec{x})$ , we apply an identical pair of pressures  $f_1(\vec{x}) = F_0 w_1(\vec{x})$  at opposite sides of Layer I, and force  $f_s(x, y) = F_0 w_s(\vec{x})$  onto the coating-substrate interface (along the  $-z$  direction), as shown in Fig. 1. The same strain and stress as in Eqs. (73) and (74) are driven by  $\tilde{f}_1$ , which are only non-vanishing within layer I. On the other hand,  $\tilde{f}_s$  drives uniform strain and stress over the entire coating, with non-vanishing components of stress and strain given by,

$$\|\tilde{T}_{ij}\| = \frac{\tilde{w}_s(1 - \sigma_s - 2\sigma_s^2) Y_c}{(1 + \sigma_c) \kappa^2 Y_s} \begin{bmatrix} \frac{k_x^2 + \sigma_c k_y^2}{1 - \sigma_c} & k_x k_y & 0 \\ k_x k_y & \frac{\sigma_c k_x^2 + k_y^2}{1 - \sigma_c} & 0 \\ 0 & 0 & 0 \end{bmatrix} \quad (82)$$

$$\|\tilde{S}_{ij}\| = -\frac{\tilde{w}_s(1 - \sigma_s - 2\sigma_s^2)}{\kappa^2 Y_s} \begin{bmatrix} k_x^2 & k_x k_y & 0 \\ k_x k_y & k_y^2 & 0 \\ 0 & 0 & -\sigma_c \end{bmatrix} \quad (83)$$

where Young's modulus  $Y_c$  and Poisson's ratio  $\sigma_c$  of the coating are given by values within layer I. The total dissipation in

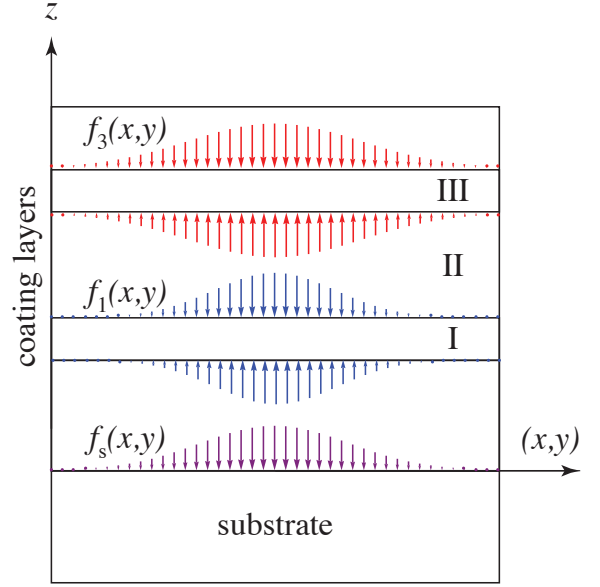


Figure 2: Illustrations of forces applied onto various interfaces within the coating. Each of Layers I and III in the coating are assumed to be uniform (but they might each contain a different kind of material); region II denotes the entire gap between them, which may well contain many different dielectric layers. A pair of force distribution  $f_1$  ( $f_3$ ) with the same pressure profile but in opposite directions is exerted on opposite sides of Layer I (III), while  $f_s$  is exerted on the coating-substrate interface. (Although each pair has the same pressure profile, they may be different from each other.) The three distributions may well have different profiles (as also illustrated in the figure).

this case will have the following structure,

$$\frac{W_{\text{diss}}}{F_0^2} = l_1 \left[ W_{11} \int w_1^2 d^2 \vec{x} + 2W_{1s} \int w_1 w_s d^2 \vec{x} + W_{ss} \int w_s^2 d^2 \vec{x} \right], \quad (84)$$

with the first term arising from dissipation in layer I that is due to strain and stress driven by  $f_1$ , the second term also arising from dissipation in layer I arising from cross terms between strains and stresses caused by  $f_1$  and  $f_s$ , and the third term arises from dissipations throughout the entire coating, due to strain and stress caused by  $f_s$ . Here  $W_{11}$  is the same as defined by Eq. (78), and

$$W_{js} = \frac{(1 - \sigma_s - 2\sigma_s^2)(1 - \sigma_j - 2\sigma_j^2)}{2(1 - \sigma_j)^2 Y_s} (\phi_B^j - \phi_S^j) \quad (85a)$$

$$W_{ss}^{(j)} = \frac{(1 - \sigma_s - 2\sigma_s^2)^2 Y_j}{(1 - \sigma_j)^2 Y_s^2} \left[ \frac{1 - 2\sigma_j}{2} \phi_B^j + \frac{1 - \sigma_j + \sigma_j^2}{1 + \sigma_j} \phi_S^j \right] \quad (85b)$$

Note that we have added a superscript ( $j$ ) for  $W_{ss}$  to indicate that here the dissipation is due to the pair of forces applied on one thin layer alone.

Here again, the dependences on  $w_1^2$  and  $w_s^2$  indicates that fluctuations at different transverse locations,  $\vec{x} \neq \vec{x}'$ , are uncorrelated, while the  $l_1$  in front of  $W_{11}$ , and the arbitrariness of  $l_1$  means that  $S_{zz}$  fluctuations at different  $z$  locations within

the thin layers are uncorrelated. The  $l_1$  in front of both  $W_{1s}$  and  $W_{ss}$  indicates that all  $S_{zz}$  within layer I are correlated with  $z_s$ , the same way, even though all of them are mutually uncorrelated.

This allows us to extract the following

$$S_{z_s z_s}(\vec{x}, \vec{x}') = \frac{4k_B T}{3\pi f} \delta^{(2)}(\vec{x} - \vec{x}') \sum_j l_j W_{ss}^{(j)} \quad (86a)$$

$$S_{S_{zz} z_c}(\vec{x}, \vec{x}', z') = \frac{4k_B T}{3\pi f} \delta^{(2)}(\vec{x} - \vec{x}') W_{js}. \quad (86b)$$

Here for Eq. (86b),  $j$  is the layer with which  $z'$  is associated; and this labeling is to help identify which material parameter to use in  $W_{js}$ .

### C. The anatomy of coating thermal noise

Here let us assemble Eqs. (81), (86a) and (86b) from the previous sections, and write:

$$S_{S_{zz} S_{zz}}^{ij}(\vec{x}, z; \vec{x}', z') = \frac{4k_B T}{3\pi f} \frac{(1 + \sigma_j)(1 - 2\sigma_j)}{Y_j(1 - \sigma_j)^2} \left[ \frac{1 + \sigma_j}{2} \phi_{Bj} + (1 - 2\sigma_j) \phi_{Sj} \right] \delta_{ij} \delta^{(2)}(\vec{x} - \vec{x}') \delta(z - z') \quad (87a)$$

$$S_{z_s z_s}(\vec{x}, \vec{x}') = \frac{4k_B T}{3\pi f} \frac{(1 - \sigma_s - 2\sigma_s^2)^2}{Y_s^2} \sum_j \frac{Y_j l_j}{(1 - \sigma_j)^2} \left[ \frac{1 - 2\sigma_j}{2} \phi_{Bj} + \frac{1 - \sigma_j + \sigma_j^2}{1 + \sigma_j} \phi_{Sj} \right] \delta^{(2)}(\vec{x} - \vec{x}') \quad (87b)$$

$$S_{z_s S_{zz}}(\vec{x}, \vec{x}', z') = \frac{2k_B T}{3\pi f} \frac{(1 - \sigma_s - 2\sigma_s^2)(1 - \sigma_j - 2\sigma_j^2)}{Y_s(1 - \sigma_j)^2} [\phi_{Bj} - \phi_{Sj}] \delta^{(2)}(\vec{x} - \vec{x}') \quad (87c)$$

Here we have assumed that  $z$  belongs to the  $i$ -th layer and that  $z'$  belongs to the  $j$ -th layer, respectively. The thickness fluctuation of different layers are mutually independent [note the Kronecker delta in Eq. (87a)], while the thickness fluctuation of each layer is correlated with the height fluctuation of the coating-substrate interface [Eq. (87c)].

Fluctuations in the strain  $S_{zz}$  and the coating-substrate interface  $z_s$ , described by Eqs. (87a)–(87b), can be represented alternatively as being driven by a number of independent fluctuating fields that exist throughout the coating. Such a representation allows us to better appreciate the origin and the magnitude of these fluctuations.

In order to do so, let us first define  $3N$  thermal noise fields (i.e., 3 for each coating layer),  $n_j^B(\mathbf{x})$ ,  $n_j^{S_A}(\mathbf{x})$  and  $n_j^{S_B}(\mathbf{x})$ , all independent from each other, with

$$S_{n_j^B n_k^B} = \frac{4k_B T(1 - \sigma_j - 2\sigma_j^2)}{3\pi f Y_j(1 - \sigma_j)^2} \phi_B^j \delta_{jk} \delta^{(3)}(\mathbf{x} - \mathbf{x}'), \quad (88a)$$

$$S_{n_j^{S_A} n_k^{S_A}} = S_{n_j^{S_B} n_k^{S_B}} = \frac{4k_B T(1 - \sigma_j - 2\sigma_j^2)}{3\pi f Y_j(1 - \sigma_j)^2} \phi_S^j \delta_{jk} \delta^{(3)}(\mathbf{x} - \mathbf{x}'), \quad (88b)$$

and all other cross spectra vanishing. Here  $j$  labels coating layer, the superscript  $B$  indicates bulk fluctuation, while  $S_A$  and  $S_B$  label two types of shear fluctuations. The normalization of these fields are chosen such that each of these fields, when integrated over a length  $l_j$  along  $z$ , have a noise spectrum that is roughly the same magnitude as a single-layer thermal noise.

Noise fields  $n_j^B(\mathbf{x})$ ,  $n_j^{S_A}(\mathbf{x})$  and  $n_j^{S_B}(\mathbf{x})$  can be used to generate thickness fluctuations of the layers and the interface fluctua-

	Thickness ( $\delta_j$ )	Surface height ( $z_s$ )
Bulk	$C_j^B = \sqrt{\frac{1 + \sigma_j}{2}}$	$D_j^B = \frac{1 - \sigma_s - 2\sigma_s^2}{\sqrt{2(1 + \sigma_j)}} \frac{Y_j}{Y_s}$
Shear A	$C_j^{S_A} = \sqrt{1 - 2\sigma_j}$	$D_j^{S_A} = -\frac{1 - \sigma_s - 2\sigma_s^2}{2\sqrt{1 - 2\sigma_j}} \frac{Y_j}{Y_s}$
Shear B	(none)	$D_j^{S_B} = \frac{\sqrt{3}(1 - \sigma_j)(1 - \sigma_s - 2\sigma_s^2)}{2\sqrt{1 - 2\sigma_j}(1 + \sigma_j)} \frac{Y_j}{Y_s}$

Table I: Transfer functions from bulk and shear noise fields to layer thickness and surface height.

tion (87a)–(87b) if we define

$$u_{zz}(\vec{x}, z) = C_j^B n_j^B(\vec{x}, z) + C_j^{S_A} n_j^{S_A}(\vec{x}, z) \quad (89)$$

and

$$z_s(\vec{x}) = \sum_j \int_{L_{j+1}}^{L_j} dz \left[ D_j^B n_j^B(\vec{x}, z) + D_j^{S_A} n_j^{S_A}(\vec{x}, z) + D_j^{S_B} n_j^{S_B}(\vec{x}, z) \right] \quad (90)$$

For each coating layer,  $C_j^B$  and  $D_j^B$  are transfer functions from the bulk noise field  $n_j^B$  to its own thickness  $\delta l_j$  and to surface height  $z_s$ , respectively;  $C_j^{S_A}$  and  $D_j^{S_A}$  are transfer functions from the first type of shear noise to thickness and surface height; finally  $D_j^{S_B}$  is the transfer function from the second type of shear noise to surface height (note that this noise field does not affect layer thickness). Explicit forms of these transfer functions are listed in Table. I.

Equations (89) and (90) owe their simple forms to the underlying physics of thermal fluctuations:

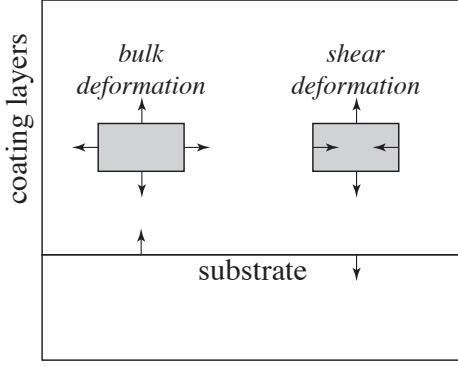


Figure 3: Illustration of the correlations between coating thickness  $\delta l_j$  and the height of the coating-substrate interface,  $z_s$ . On the left, for a bulk deformation: when a coating element is expanding, its expansion along the  $x$ - $y$  plane lifts the coating-substrate interface upwards, causing additional motion of the coating-air interface correlated to that caused by the increase in coating thickness. On the right, a particular shear mode: when a coating element is expanding, its contraction along the  $x$ - $y$  plane pushes the coating-substrate interface downwards, causing addition motion of the coating-air interface anti-correlated to that caused by the increase in coating thickness.

For *bulk noise*, i.e., terms involving  $n_j^B$ , the form of Eqs. (89) and (90) indicates that the interface fluctuation due to bulk dissipation is simply a sum of pieces that are directly proportional to the bulk-induced thickness fluctuations of each layer. This means the thermal bulk stress in a layer drive simultaneously the thickness fluctuation of that layer and a fluctuation of the coating-substrate interface. The fact that  $D_j^B$  and  $C_j^B$  having the same sign means that when thickness increases, the interface also rises (with intuitive explanation shown in Figure 3). This sign of correlation is generally unfavorable because the two noises add constructively towards the rise of the coating-air interface.

For *shear noise*, the situation is a little more complicated, because unlike bulk deformations, there are a total of 5 possible shear modes. From Eq. (73) and (74), it is clear that  $f_1$ , applied on opposites of Layer I (Figure 2), only drives the  $xx + yy - 2zz$  shear mode and the  $xx + yy + zz$  bulk mode, while from Eq. (82) and (83), the force distribution  $f_s$  drives three shear modes of  $xx - yy$ ,  $xy + yx$ , and  $xx + yy - 2zz$ . This means while thermal shear stresses in the  $xx + yy - 2zz$  mode drives layer thickness and interface fluctuation simultaneously, there are additional modes of shear stress,  $xx - yy$  and  $xy + yx$ , that only drives the interface without driving layer thickness. Our mode  $S_A$ , which drives both layer thickness and interface height, therefore corresponds to the physical shear mode of  $xx + yy - 2zz$ ; our mode  $S_B$ , which only drives interface height, corresponds to the joint effect of the physical shear modes  $xx - yy$  and  $xy + yx$ . It is interesting to note that for  $S_A$ , its contributions to  $\delta l_j$  and  $z_s$  are anti correlated, because  $C^{S_A}$  and  $D^{S_A}$  have opposite signs. This is intuitively explained in Fig. 3.

As an example application of Eqs. (89) and (90), if we ignore light penetration into the coating layers, namely, when

thermal noise is equal to

$$\xi^{\text{np}} \equiv -z_s - \sum_j \delta l_j \quad (91)$$

we have

$$\begin{aligned} \xi^{\text{np}} = - \sum_j \int_{L_j}^{L_{j+1}} dz & \left[ (C_j^B + D_j^B) n_j^B \right. \\ & + (C_j^{S_A} + D_j^{S_A}) n_j^{S_A} \\ & \left. + D_j^{S_B} n_j^{S_B} \right] \quad (92) \end{aligned}$$

in which contributions from each layer has been divided into three mutually uncorrelated groups, each arising from a different type of fluctuations. Here we see explicitly that  $C^B$  and  $D^B$  sharing the same sign increases contributions from  $n^B$ ,  $C^{S_A}$  and  $D^{S_A}$  having opposite signs suppresses contributions from  $n^{S_A}$ .

Finally, we note that in the spectral density of  $\xi^{\text{np}}$ , contributions directly from coating thickness will be proportional to  $|C_j^B|^2$  and  $|C_j^{S_A}|^2$ , and hence proportional to  $1/Y_c$ , those from interface height will be  $|D_j^B|^2$ ,  $|D_j^{S_A}|^2$  and  $|D_j^{S_B}|^2$ , and hence proportional to  $Y_c/Y_s^2$ , while those from correlations will be proportional to  $C_j^B D_j^B$  and  $C_j^{S_A} D_j^{S_A}$ , and hence proportional to  $1/Y_s$ . This confirms our anticipation at the end of Sec. III D.

#### D. Full formula for thermal noise

Now we give the complete formulas for amplitude and phase noise spectrum [Cf. Eq. (94) and Eq. (95)]. As we consider light penetration into the coating, we resort to Eq. (24), and write:

$$\begin{aligned} \xi(\vec{x}) - i\zeta(\vec{x}) &= - \sum_j \int_{z_{j+1}}^{z_j} dz \left\{ \left[ 1 + \frac{i\epsilon_j(z)}{2} \right] C_j^B + D_j^B \right\} n_j^B(\vec{x}, z) \\ &+ \left[ \left[ 1 + \frac{i\epsilon_j(z)}{2} \right] C_j^{S_A} + D_j^{S_A} \right] n_j^{S_A}(\vec{x}, z) \\ &+ D_j^{S_B} n_j^{S_B}(\vec{x}, z) \left. \right\} \quad (93) \end{aligned}$$

Here spectra of independent fields  $n_j^B$ ,  $n_j^{S_A}$  and  $n_j^{S_B}$  have been given in Eqs. (88a)–(88b),  $\epsilon$  is defined in Eq. (25), while the transfer functions  $C$ 's and  $D$ 's are listed in Table I.

We can then obtain the spectrum of phase noise (after averaging over the mirror surface, weighted by the power profile

of the optical mode) as

$$\begin{aligned}
S_{\bar{\xi}} &= \sum_j \int_{z_{j+1}}^{z_j} \frac{dz}{\lambda_j} \left[ \left[ 1 - \text{Im} \frac{\epsilon_j(z)}{2} \right] C_j^B + D_j^B \right]^2 S_j^B \\
&+ \sum_j \int_{z_{j+1}}^{z_j} \frac{dz}{\lambda_j} \left[ \left[ 1 - \text{Im} \frac{\epsilon_j(z)}{2} \right] C_j^{S_A} + D_j^{S_A} \right]^2 S_j^S \\
&+ \sum_j \left[ D_j^{S_B} \right]^2 \frac{l_j}{\lambda_j} S_j^S \\
&\equiv \sum_j q_j^B S_j^B + q_j^S S_j^S
\end{aligned} \tag{94}$$

and spectrum of amplitude noise as

$$\begin{aligned}
S_{\bar{\xi}} &= \sum_j \int_{z_{j+1}}^{z_j} \frac{dz}{\lambda_j} \left\{ \left[ C_j^B \text{Re} \frac{\epsilon_j(z)}{2} \right]^2 S_j^B \right. \\
&\quad \left. + \left[ C_j^{S_A} \text{Re} \frac{\epsilon_j(z)}{2} \right]^2 S_j^S \right\}
\end{aligned} \tag{95}$$

Here  $\lambda_j$  is the wavelength of light in Layer  $j$ , and we have defined

$$S_j^X \equiv \frac{4k_B T \lambda_j \phi_X^j (1 - \sigma_j - 2\sigma_j^2)}{3\pi f Y_j (1 - \sigma_j)^2 \mathcal{A}_{\text{eff}}}, \quad X = B, S. \tag{96}$$

which is at the level of coating thickness fluctuation of a single layer of dielectrics with material parameters identical to layer  $j$  and length equal to  $\lambda_j$ . Note that the quantity  $S_j^X$  only depends on the material properties (and temperature) of the layer, and is independent from length of that layer; the quantities  $q_j^X$  (see Fig. 7), on the other hand, give us the relative thermal-noise contribution of each layer in a dimensionless way.

Note that the reason for keeping the integrals in Eqs. (94) and (95) is because  $\epsilon$  has a  $z$  dependence, which originates from the fact that the back-scattering contributions to  $\delta\phi_j$ 's and  $\delta r_j$ 's a weighted integral of  $u_{zz}$  within each layer [Cf. (17) and (18)].

## V. EFFECT OF LIGHT PENETRATION INTO THE COATING

In this section, we synthesize results from Sec. II and Sec. IV, and compute the full Brownian thermal noise for coating configurations. We will illustrate how the light penetration affects the total noise in highly reflective coatings.

### A. Optics of multi-layer coatings

For completeness of the paper, we briefly review how light penetration coefficient  $\partial \log \rho / \partial \phi_j$  can be calculated.

From an interface from layer  $i$  to  $j$  (here  $j$  is either  $i + 1$  or  $i - 1$ ), we denote the reflectivity and transmissivity of different

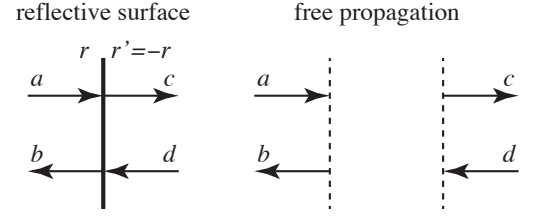


Figure 4: Two basic transformations involved in solving for optical fields in a multi-layer coating.

Parameter	Tantala(Ti <sub>2</sub> O <sub>5</sub> )	Silica(SiO <sub>2</sub> )
Refractive index	2.07 [22]	1.45 [22]
Poisson's ratio	0.23 [23]	0.17[23]
Young's modulus (Pa)	$1.4 \times 10^{11}$ [24]	$7 \times 10^{10}$ [23]
Loss angle ( $\phi_B = \phi_S$ )	$2.3 \times 10^{-4}$ [25]	$4.0 \times 10^{-5}$ [26]
Photoelastic coefficient	-0.50 [27]	-0.41[28]

Table II: Baseline material parameters.

layers by  $r_{ij}$  and  $t_{ij}$ :  $r_{ij}^2 + t_{ij}^2 = 1$ .

$$r_{ij} = \frac{n_i - n_j}{n_i + n_j} \tag{97}$$

We also define  $n_{N+1} = n_1$ , since that is the refractive index of the substrate.

A matrix approach can be applied to solve for the amplitude of light inside the layers, when we view the coating as made up from two elementary transformations, each representable by a matrix. In this approach, instead of writing out-going fields in terms of in-going fields, one writes fields to the right of an optical element in terms of those to the left. As illustrated in Figure 4, for reflection at an interface (left panel), we write

$$\begin{bmatrix} c \\ d \end{bmatrix} \equiv \mathbf{R}_r = \frac{1}{t} \begin{bmatrix} 1 & -r \\ -r & 1 \end{bmatrix} \begin{bmatrix} a \\ b \end{bmatrix} \tag{98}$$

On the other hand, for propagation across a gap with phase shift  $\phi$ , we have

$$\begin{bmatrix} c \\ d \end{bmatrix} \equiv \mathbf{T}_\phi = \begin{bmatrix} e^{i\phi} & 0 \\ 0 & e^{-i\phi} \end{bmatrix} \begin{bmatrix} a \\ b \end{bmatrix} \tag{99}$$

In this way, assuming the input and output field amplitude at the top surface of a multi-layer coating to be  $v_1$  and  $v_2$ , and writing those right inside the substrate to be  $s_1$  and  $s_2$ , we have

$$\begin{bmatrix} s_1 \\ s_2 \end{bmatrix} = \begin{bmatrix} M_{11} & M_{12} \\ M_{21} & M_{21} \end{bmatrix} \begin{bmatrix} v_1 \\ v_2 \end{bmatrix} = \mathbf{M} \begin{bmatrix} v_1 \\ v_2 \end{bmatrix} \tag{100}$$

where  $\mathbf{M}$  is given by

$$\mathbf{M} = \mathbf{R}_{r_{N,N+1}} \mathbf{T}_{\phi_{N-1}} \mathbf{R}_{r_{N-1,N}} \cdots \mathbf{R}_{r_{12}} \mathbf{T}_{\phi_1} \mathbf{R}_{r_{01}} \tag{101}$$

The complex reflectivity is given by

$$\rho = -M_{21}/M_{22} \tag{102}$$

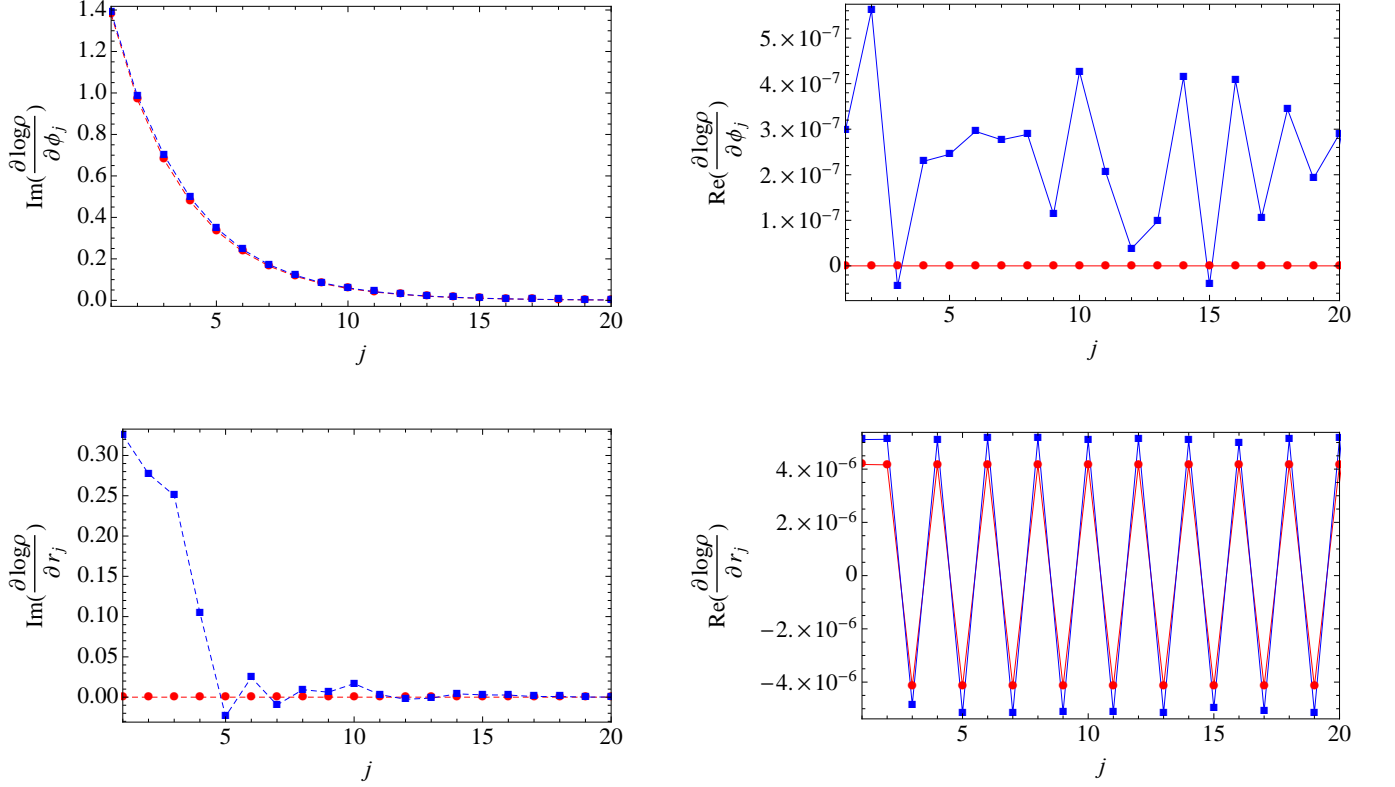


Figure 5: Real (solid curves) and imaginary (dashed curves) parts of  $\partial \log \rho / \partial \phi_j$  (upper panel) and  $\partial \log \rho / \partial r_j$  (lower panel), for conventional (red curve) and Advanced LIGO (blue curve) coatings. [Note that  $\text{Re}(\partial \log \rho / \partial \phi_j) = 0$  for conventional coating.]

### B. Levels of light penetration in Advanced LIGO ETM Coatings

In Advanced LIGO, the coating stack is made from alternating layers of two materials:  $\text{SiO}_2$  ( $n_1 = 1.45$ ) and  $\text{Ta}_2\text{O}_5$  ( $n_2 = 2.07$ ). Here we consider the End Test-mass Mirror (ETM). In order to achieve very high reflectivity, the coating is made of 19 successive pairs of alternating  $\text{SiO}_2$  and  $\text{Ta}_2\text{O}_5$  layers, all  $\lambda/4$  in thickness except the top one, which is  $\lambda/2$ . We will refer to this as the *conventional coating*. An alternative design has been made to allow the coating to operate at both 1064 nm and 532 nm. We shall refer to this as the *Advanced LIGO coating* (see Appendix. IV) [29].

In Fig. 5, we plot real and imaginary parts of  $\partial \log \rho / \partial \phi_j$  and  $\partial \log \rho / \partial r_j$  [see Eq. (13)], for both conventional and Advanced LIGO coating. Here we note that the real parts of these derivatives are at the order of  $10^{-6}$ , which means  $\bar{\zeta}$  is less than  $\bar{\xi}$  by 6 orders of magnitude. This, together with considerations in Sec. II E, will make amplitude coating noise negligible.

In Eq. (27), we have divided contributions to  $\xi$  into four terms, the first,  $z_s$ , is the height of the coating-substrate interface, while the other three are related to fluctuations in layer thickness,  $\delta l_j$ ,  $\delta l_j^c$  and  $\delta l_j^s$ , see Eqs. (27)–(30). We can illustrate the effect of light penetration by showing the relative size of these three contributions for each layer. In Figure 6, we carry out this illustration, for conventional coating on the

left panel and for Advanced LIGO coating on the right. We use a solid black line to indicate the non-photoelastic part of  $\mathcal{T}_j^{\xi}$  [i.e., terms not containing  $\beta_j$ , see Eq. (28)], and we use red-long-dashed, blue-short-dashed, and purple-dotted curves to indicate the photoelastic part of  $\mathcal{T}_j^{\xi}$ ,  $\mathcal{T}_j^{\xi c} \sqrt{\langle (\delta l_j^c)^2 \rangle / \langle (\delta l_j)^2 \rangle}$  and  $\mathcal{T}_j^{\xi s} \sqrt{\langle (\delta l_j^s)^2 \rangle / \langle (\delta l_j)^2 \rangle}$ , respectively. The weighting factors,

$$\sqrt{\langle (\delta l_j^c)^2 \rangle / \langle (\delta l_j)^2 \rangle} = \frac{1}{\sqrt{2}} \sqrt{1 + \frac{\sin 4\phi_j}{4\phi_j}}, \quad (103)$$

$$\sqrt{\langle (\delta l_j^s)^2 \rangle / \langle (\delta l_j)^2 \rangle} = \frac{1}{\sqrt{2}} \sqrt{1 - \frac{\sin 4\phi_j}{4\phi_j}}, \quad (104)$$

have been added for  $\mathcal{T}_j^{\xi c}$  and  $\mathcal{T}_j^{\xi s}$ , respectively, to correct for the fact that  $\delta l_j^c$  and  $\delta l_j^s$  have different r.m.s. values compared to  $\delta l$ . Because of the lack of experimental data, we have assumed  $\beta_j = -0.4$  identically. Note that in order to focus on the effect of light penetration, we have only showed the first 10 layers.

In the figure, the effect of light penetration into the coating layers is embodied in the deviation of the black solid curve from unity in the first few layers, and in the existence of the other curves. Although we cannot perceive the correlation between these contributions, we can clearly appreciate that only

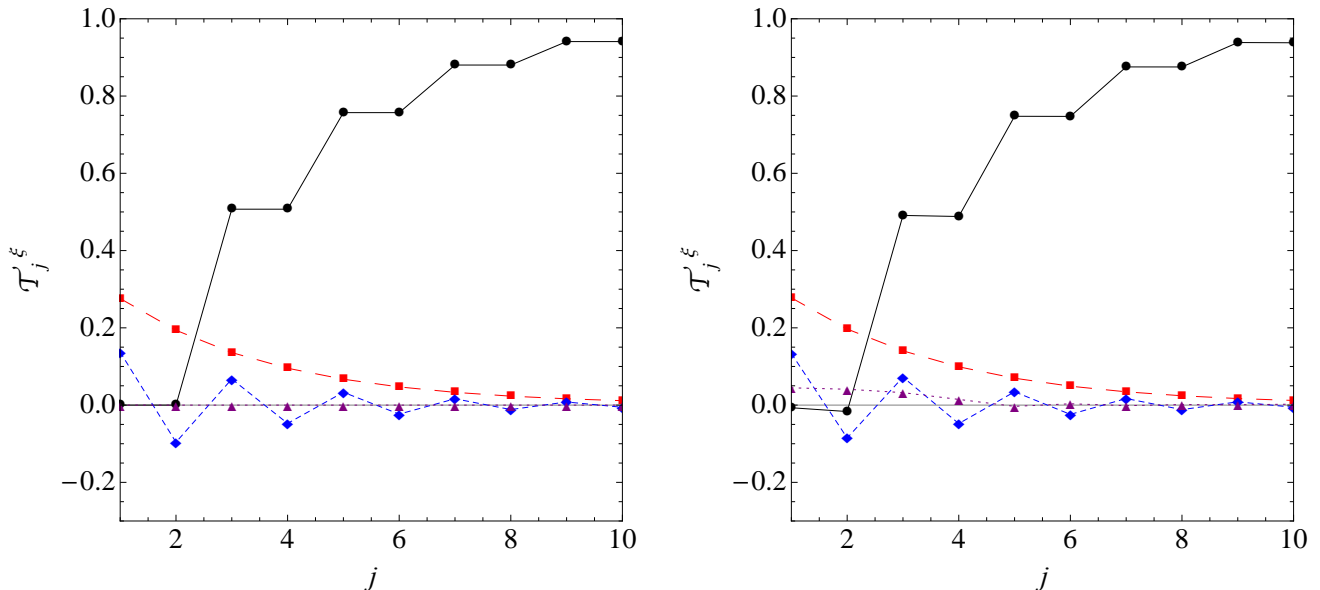


Figure 6: Light penetration into the first 10 layers of a 38-layer coating (left panel for conventional coating and right panel for Advanced LIGO coating). We plot the non-photoelastic part of  $\mathcal{T}_j$  in black solid curves, the photoelastic part of  $\mathcal{T}_j^s$  in long-dashed red curves, as well as  $\mathcal{T}_j^s$  (scaled by rms value of  $\delta l_j^c$  with respect to the rms value of  $\delta l_j$ , shown in short-dashed blue curves) and  $T_j^s$  (scaled by rms value of  $\delta l_j^s$ , shown in dotted purple curves). These plots indicate that for both structures, light penetration is restricted within the first 10 layers.

the first few layers are penetrated, and that the total effect of light penetration will be small. We should also expect the effect of photoelasticity (dashed curves) to be small, and the effect of back-scattering (which gives rise to  $\mathcal{T}_j^{\xi c}$  and  $\mathcal{T}_j^{\xi s}$ , blue and purple dashed curves) to be even smaller.

### C. Thermal noise contributions from different layers

Let us now examine the breakdown of the total coating noise by plotting the coefficients  $q_j^B$  and  $q_j^S$  in Eq. (94). In Fig. 7, we plot silica contributions on top panels, and tantala contributions on lower panels, with bulk contributions on left panels, and shear contributions on right panels. Here we use the baseline parameters shown in Table II. As it turns out, the results for conventional and Advanced LIGO coatings are hardly distinguishable from each other — therefore we only use the Advanced LIGO coating. The red curve uses  $\beta = -1$ , black uses  $\beta = 0$  and blue uses  $\beta = 1$ . Superimposed onto the solid lines are dashed lines of each type, calculated without introducing the back-scattering terms; the effect is noticeable for the first few layers.

## VI. DEPENDENCE OF THERMAL NOISE ON MATERIAL PARAMETERS

Experimental knowledge of coating materials is limited. Most notably, values of Young’s moduli and Poisson’s ratios

of the coating materials are still uncertain, while only *one combination* of the two loss angles have been experimentally measured by ring-down experiments. In this section, we explore the possible variation in coating Brownian noise, away from the baseline configuration (Table II), considering these uncertainties. We shall use the Advanced LIGO coating structure mentioned in the previous section.

### A. Dependence on Ratios Between Loss Angles

In the baseline (Table II), we have assumed that  $\phi_B$  and  $\phi_S$  are equal, but this is only out of our ignorance: experiments have only been able to determine one particular combination of these two angles. We now explore the consequence of having these loss angles not equal, while keeping fixed the combination measured by ring down rate of drum modes [see Eq. (110)].

In Figure 8, while fixing all other baseline parameters, we plot how each type of thermal noise (i.e., silica vs tantala, bulk vs shear) varies when the ratio  $\phi_B/\phi_S$  for both tantala and silica layers varies between 1/5 and 5. We use blue for tantala, red for silica, dotted for bulk, dashed for shear, and solid for the total of bulk and shear. In this configuration, tantala layers’ contribution to thermal noise always dominate over silica layers, mainly due to the higher loss angle. As we vary the ratio between the loss angles, there is moderate variation of thermal noise. For the dominant tantala, as  $\phi_B/\phi_S$  vary from 1/5 to 5, there is a 30% change in thermal noise, while for



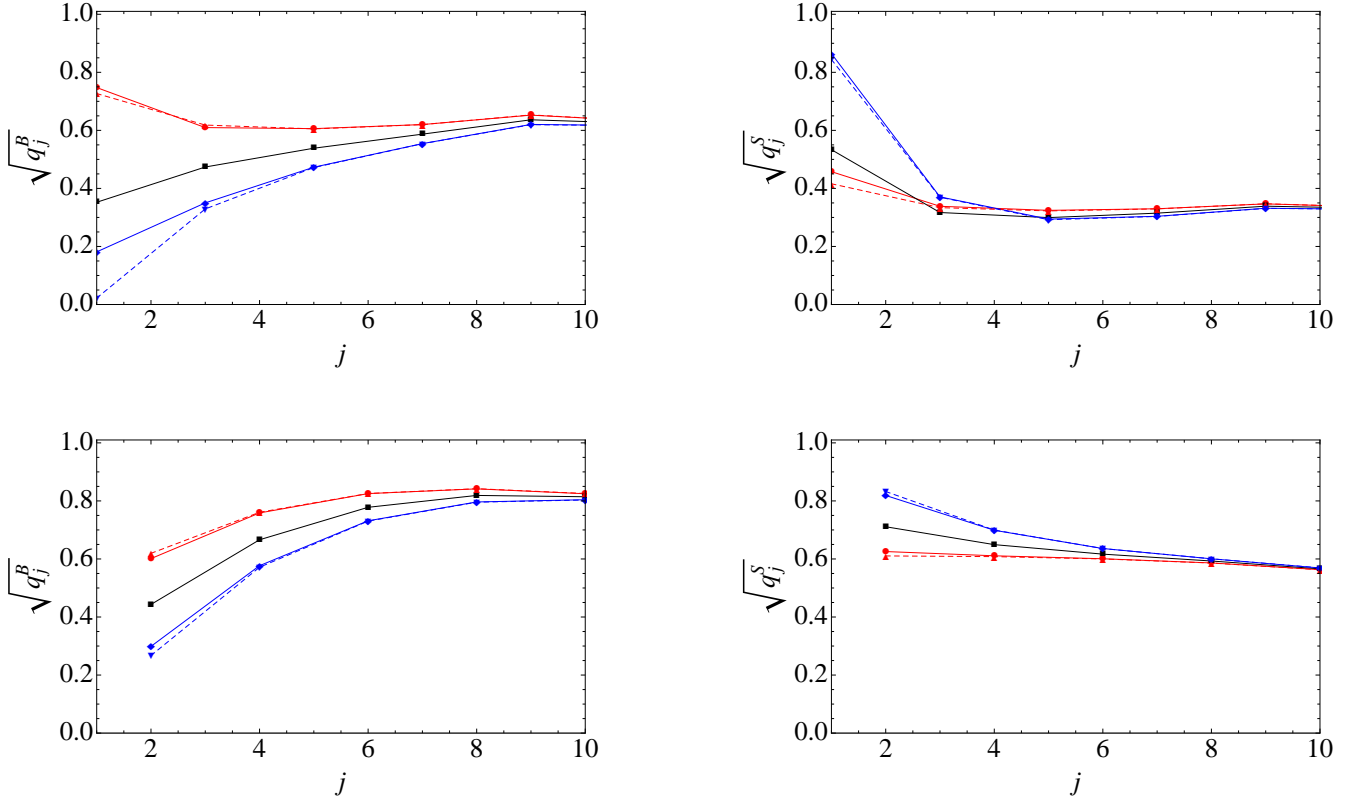


Figure 7: A break-down of thermal noise contributions from silica (upper panels) and tantala (lower panels) layers, from bulk (left panels) and shear (right panels) losses. Blue curves correspond to  $\beta = -1$ , black  $\beta = 0$  and red  $\beta = 1$ . Dashed curves indicate results calculated without including back-scattering effects.

silica, the change is a more significant 68%.

As we see from Fig. 8, a larger value of  $\phi_B/\phi_S$  gives rise to higher bulk, lower shear, and higher total noise — this is reasonable because bulk fluctuations drive correlated noise between layer’s thickness and the height of coating-substrate interface, while shear fluctuations drive anti-correlated noise, as shown in Fig. 3.

Moreover, the fact that variation is more significant for silica layers can be explained when we recall that thickness-induced thermal noise is proportional to  $1/Y_c$ , while surface-height-induced thermal noise is proportional to  $Y_c/Y_s^2$ . For silica layers,  $Y_c$  is assumed to be equal to  $Y_s$ , so the two types of noise being added (bulk) or subtracted (shear) are more comparable in magnitude; by contrast, the Young’s modulus of tantala layers is significantly higher than that of the substrate, causing the noise to be dominated by fluctuations of the height of the coating-substrate interface, therefore making correlations between the two types of noise less important.

In Fig. 9, we plot variations in the total noise as we vary  $\phi_B/\phi_S$  for silica layers (blue) or tantala layers (red) only, and fix the other one. It shows that the variance of tantala’s loss angle will generate larger change of the total noise.

## B. Dependence on Young’s moduli and Poisson’s ratios

Since the Young’s modulus and Poisson’s ratios of coating materials, especially of tantala, are also uncertain. In Fig. 10, we plot variations of tantala thermal noise when its Young’s modulus varies from the baseline value by up to a factor of 2, for  $\phi_B/\phi_S = 0.2, 0.5, 1, 2$  and 5. The noise is seen to vary by  $\sim 15\%$  as Young’s modulus varies by a factor of  $\sim 2$ .

We can also explain the way the thermal noise varies as a function of  $Y_c$ . Starting from the baseline value, a lower  $Y_c$  leads to a lower thermal noise, until  $Y_c$  becomes comparable to  $Y_s$  (which we fix at the baseline value, equal to  $0.5Y_{Ta}$ ), and starts to increase again. Such a behavior is reasonable because thickness noise spectrum and interface noise spectrum are proportional to  $\sim 1/Y_c$  and  $\sim Y_c/Y_s^2$ , respectively — as we decrease  $Y_c$  from the baseline  $Y_{Ta}$  value, we transition from interface fluctuation being dominant towards equal amount of both noises (which gives a minimum total noise), and then towards thickness fluctuation becoming dominant.

In Fig. 11, we explore the effect of varying coating Poisson’s ratio, for the same values of  $\phi_B/\phi_S$  chosen in Fig. 10. In the baseline assumption of  $\phi_B = \phi_S$ , when bulk and shear have the same level of loss, thermal noise does not depend much on Poisson’s ratio. However, if  $\phi_B/\phi_S$  turns out to differ significantly from 1, and if Poisson’s ratio can be larger than the baseline value by more than  $\sim 0.1$ , then thermal noise can



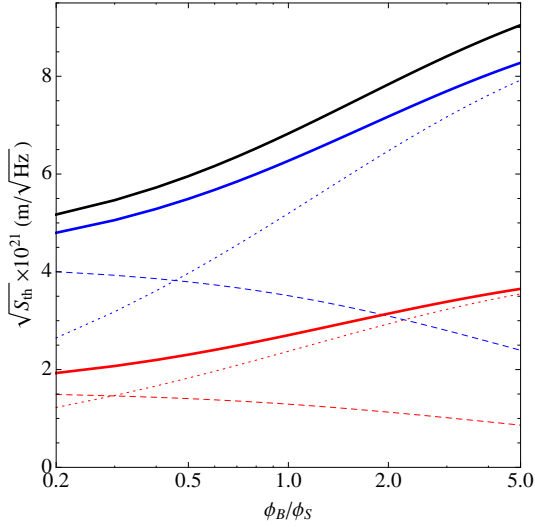


Figure 8: (Color Online) Variations in thermal noise contributions when  $\phi_B/\phi_S$  is varied. Contributions from tantala layers is shown in blue, those from silica layers are shown in red. The total thermal noise is in black. Bulk contributions are shown in dotted curves, while shear contributions are shown in dashed curves.

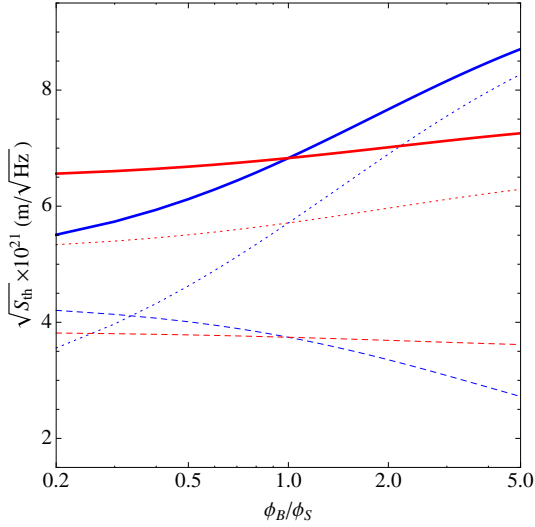


Figure 9: (Color Online) Variations in total noise when  $\phi_B/\phi_S$  is varied: (solid) total noise, (dotted) total bulk noise, (dashed) total shear noise. The red (blue) curve corresponds to only varying  $\phi_B/\phi_S$  for tantala (silica). With  $\phi_B/\phi_S$  of tantala or silica varying from 0.2 to 5, the change in total noise is 58.1% and 10.6% respectively.

vary by  $\sim 10\%$ .

### C. Dependence on Photoelastic Coefficients

Photoelastic properties of the coating materials are not yet well known. In Fig. 12, we plot the fractional change in thermal noise, separately for silica (left panel) and tantala (right

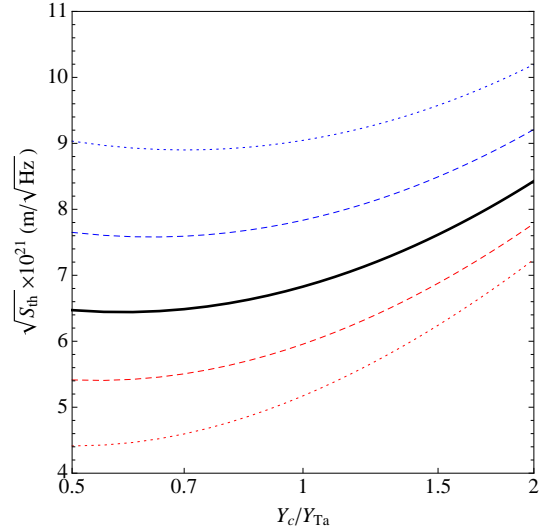


Figure 10: Thermal noise contribution from tantala, as its Young's modulus deviates from baseline value, for  $\phi_B/\phi_S=5$  (blue dashed), 2 (blue dotted), 1 (black solid), 1/2 (red dotted), and 1/5 (red dashed).

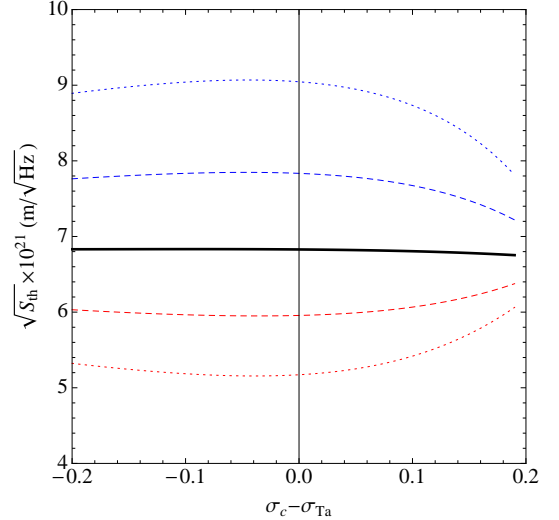


Figure 11: Thermal noise contribution from tantala, as its Poisson's ratio deviates from baseline value, for  $\phi_B/\phi_S=5$  (blue dashed), 2 (blue dotted), 1 (black solid), 1/2 (red dotted), and 1/5 (red dashed).

pane), and for bulk (blue) and shear (red) losses, when we vary  $\beta$  between -1 and +1. Dashed curves are obtained ignoring back-scattering effects.

It is interesting to note that for small values of  $\beta$ , the dependence of noise on  $\beta$  have different trends for bulk and shear contributions. This is also related to the different types of correlations between thickness and interface height fluctuations. As we can see from the Figure, the effect of varying  $\beta$  is small, since it only affects thermal noise due to light penetration into the first few layers. If bulk and shear losses are indeed comparable, then cancelation between these two types of noises (especially for the more lossy tantala layers) will likely make the photo elastic effect completely negligible. Even in the case

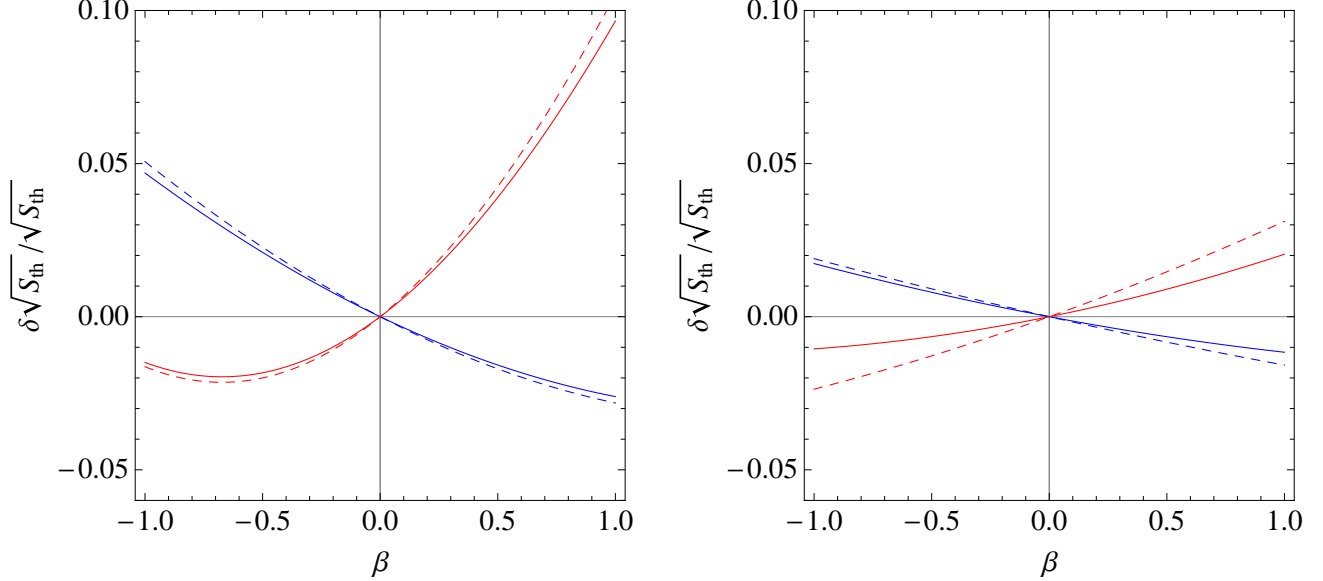


Figure 12: Fractional change in the contribution to thermal noise from all silica layers (left panel) and all tantala layers (right panel), due to bulk (blue) and shear (red) loss. Dashed lines indicate results calculated without including back-scattering terms.

when one particular type of loss dominates shall we expect at most  $\sim 2\%$  contribution from photo elasticity of the more lossy tantala — if we further assume that  $|\beta| \sim 1$  [right panel of Fig. 12].

#### D. Optimization of Coating Structure

Although a standard highly reflective coating consists of  $\lambda/4$  layers of alternating material capped by a  $\lambda/2$  layer, this structure can be modified to lower thermal noise while still maintaining a high reflectivity for the 1064 nm carrier light, e.g., as shown by Agresti et al. [30]. As their results have indicated, for baseline coating parameters and neglecting light penetration into the coating layers [14], the optimal structure is more close to a stack of pairs of  $\lambda/8$  ( $\text{Ta}_2\text{O}_5$ ) and  $3\lambda/8$  ( $\text{SiO}_2$ ) layers, capped by a  $\lambda/2$  ( $\text{SiO}_2$ ) layer. This alternative coating structure shortens the total thickness of the more lossy tantala layers, while maintaining a high reflectivity for the light. The *Advanced LIGO type* coating given in Appendix IV, on the other hand, has been optimized considering reflectivity at both 1064 nm and 532 nm, as well as thermal noise — although light penetration into the layers have not been considered.

In this section, we carry out a numerical optimization taking penetration into account. We first fix the number  $N$  of layers ( $N$  is even, so we have  $N/2$  pairs), and then for  $N$ , we use the Lagrange multiplier method to search for the constrained minimum of  $S_{th}$ , fixing  $T_{1064}$  and  $T_{532}$ , namely the power transmissivity,  $1 - |\rho|^2$  assuming the coating is lossless, evaluated at 1064 nm and 532 nm, respectively. The quantity we seek to

minimize (or, the *cost function*) is

$$y \equiv \sqrt{S_{th}} + \mu_1 T_{1064} + \mu_2 (T_{532} - 5\%)^2 \quad (105)$$

As we vary  $\mu_1$  and  $\mu_2$  and minimizing  $y$ , we obtain the constrained minimum of  $\sqrt{S_{th}}$  for different pairs of  $(T_{532}, T_{1064})$ . The aim is to obtain a series of coating configurations with approximately 5% transitivity for 532 nm, and with minimized thermal noise for a variable 3 – 20 ppm transmissivity for 1064 nm. (Note that the choice of the cost function contains a certain level of arbitrariness.)

Since we are going to carry out minimization for a large number of multipliers over a large number of degrees of freedom, we have chosen to proceed gradually allowing only the first  $n$  pairs and last  $n$  pairs of layers to vary, while maintaining the same pair structure for  $N/2 - n$  pairs in the middle (repeating doublets). In other words, our coating structure looks like:

$$\underbrace{\quad}_{2n \text{ layers}} \quad \underbrace{\quad}_{N - 2n \text{ layers}} \quad \underbrace{\quad}_{2n \text{ layers}}$$

free      repeating pair      free

In this work, we found that it suffices to choose  $n = 2$  (which corresponds to optimizing over 10 parameters); further increasing  $n$  does not lead to noticeable improvements. During our numerical optimization, we have adopted the *downhill simplex method* [31, 32].

Results for baseline material parameters (Table. II) and  $N = 38, 40$  and  $42$  have been shown in Figure 13. This figure indicates that different numbers of layers should be chosen for different target  $T_{1064}$  – more layers are required for lower transmissivity (higher reflectivity). Overall, the optimal thermal noise varies by around  $\sim 10\%$  as for  $T_{1064}$  from

target	$N$	Resulting Coating Structure										$\sqrt{S_{\text{th}}^{\text{opt}}}$			$\sqrt{S_{\text{th}}^{\lambda/4}}$
		First 4 layers				Repeated Pair		Last 4 layers				$\frac{\phi_B}{\phi_S} = \frac{1}{5}$	$\frac{\phi_B}{\phi_S} = 1$	$\frac{\phi_B}{\phi_S} = 5$	
1/5	42	0.0479	0.1581	0.3430	0.1760	0.2919	0.1897	0.3164	0.1738	0.3178	0.1627	<b>5.01</b>	6.64	8.81	5.35
1	42	0.1020	0.1250	0.3267	0.1917	0.2911	0.1914	0.3110	0.1752	0.3196	0.1609	5.02	<b>6.64</b>	8.81	7.05
5	42	0.1118	0.0968	0.3353	0.1882	0.2893	0.1939	0.3135	0.1673	0.3199	0.1662	5.02	6.64	<b>8.81</b>	9.33

Table III: Results of coating-structure optimization. We list optimized coating structures for  $T_{1064} = 5$  ppm and  $T_{532} = 5\%$ , for three target values of  $\phi_B/\phi_S$  while fixing the measured effective loss angle  $\phi_D$  [Eq. (56)] and other baseline material parameters [Table II]. Thickness of coating layers are given in units of wavelength (for 1064 nm light). For each optimized coating structure, thermal noise is calculated separately for the same three values of  $\phi_B/\phi_S$ , and given in units of  $10^{-21}$  m/  $\sqrt{\text{Hz}}$  (thermal noise for the target  $\phi_B/\phi_S$  is given in boldface, and boldface numbers should be the minimum within its column); thermal noise spectra of the 38-layer  $\lambda/4$  stack assuming the target  $\phi_B/\phi_S$  are also listed for comparison.

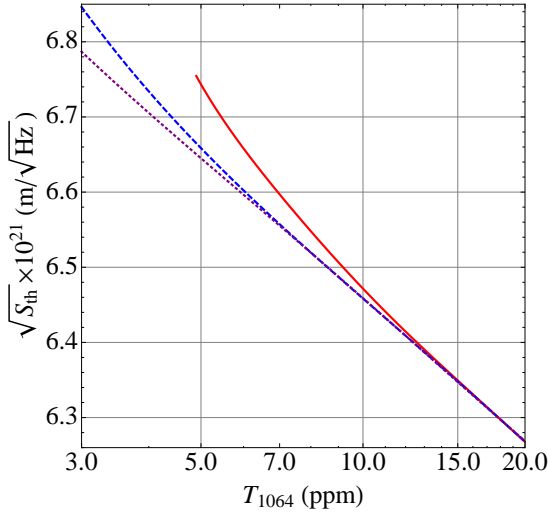


Figure 13: Optimized thermal noise versus transmissivity at 1064 nm, for a coating of 38 (red), 40 (blue), and 42 (purple) layers.

3 to 20 ppm. In particular, for the standard Advanced LIGO requirement of 5 ppm (see first column of Table III), 42 layers are found to be optimal. This is 2 more pairs or 4 more layers than the 38-layer  $\lambda/4$  doublet, which has the minimum number of layers to reach 5 ppm. The larger number of layers here gets lower thermal noise (by 6%) because the more lossy tantala layers are shortened, and the less lossy silica layers lengthened.

We have further optimized the structure when the ratio  $\phi_B/\phi_S$  is different from 1, while keeping fixed the effective loss angle measured so far — as done in Sec. VIA. For  $T_{1064} = 5$  ppm, we have listed results of optimized coating structure and thermal noise in the second and third columns of Table III. The extent of variation found here is comparable to those obtained in Sec. VIA using a standard coating structure without optimization: the optimal coating structures consistently lower thermal noise by about 6%. In addition, as shown in Table III, the optimal coating structure is robust against changes in  $\phi_B/\phi_S$ : structure obtained for any one of the values of the ratio is already almost optimal for all other ratios.

## VII. MEASUREMENTS OF LOSS ANGLES

In this section, we study possible mechanical ringdown experiments that can be used to measure independently the bulk and shear loss angles,  $\phi_B$  and  $\phi_S$  of a coating material.

In a ringdown experiment, a sample with a high intrinsic  $Q$  is coated with a thin layer of the coating material in question. Due to the mechanical losses in the coating, the quality factor of the mechanical eigenmodes of the sample will be reduced [33, 34]. More specifically, for the  $n^{\text{th}}$  eigenmode with resonant frequency  $f_n$ , if an e-folding decay time of  $\tau_n$  is measured, then the quality factor is

$$Q_n = \pi f_n \tau_n, \quad (106)$$

while correspondingly, the loss angle is given by

$$\phi(f_n) = 1/Q_n, \quad (107)$$

which is equal to the fraction of energy dissipated per radian.

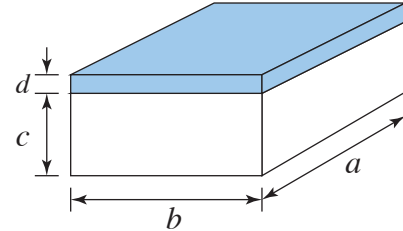


Figure 14: Rectangular shaped thin plate ( $a \times b \times c$ ) with thin coating (thickness  $d$ ):  $c \ll a, b; d \ll c$ . The transverse vibration mode is considered in this case

### A. Bending Modes of a Thin Rectangular Plate

Figure 14 shows the schematic geometry of a rectangularly shaped sample, in which a thin coating layer with thickness  $d$  is deposited on a rectangular plate with dimensions  $a \times b \times c$  ( $c \ll a, b$ ), and  $d$  is much less than  $c$ . If we pay attention only to the bending (or, in other words, flexing) oscillations of the plate, the amount of energy stored in the coating layer, in the

form of bulk and shear energies  $U_B$  and  $U_S$ , as a fraction of the entire energy  $U$ , can be calculated as

$$\frac{U_B}{U} = \frac{d Y_c (1 - \sigma_s^2)(1 - 2\sigma_c)}{3c Y_s (1 - \sigma_c)^2} \quad (108)$$

$$\frac{U_S}{U} = \frac{2d Y_c (1 - \sigma_s^2)(1 - \sigma_c + \sigma_c^2)}{3c Y_s (1 - \sigma_c)^2(1 + \sigma_c)} \quad (109)$$

Using Eq. (58), the total loss angle of the sample is

$$\begin{aligned} \phi &= \phi_{\text{sub}} \\ &+ \frac{d Y_c}{c Y_s} \frac{1 - \sigma_s^2}{1 - \sigma_c^2} \left[ \frac{\phi_B(1 - \sigma_c - 2\sigma_c^2) + 2\phi_S(1 - \sigma_c + \sigma_c^2)}{3(1 - \sigma_c)} \right] \\ &= \phi_{\text{sub}} + \frac{|D_c|}{|D_s|} \phi_D \end{aligned} \quad (110)$$

It is not surprising that only the 2-D flexural rigidity  $D$  and its imaginary part appear in Eq. (110). During the bending of a thin plate with thin coating, both the substrate and the coating are described by the 2-D flexural rigidity, first introduced in Sec. III B [see Eqs. (55) and (56) and Sec. 13 of Ref. [18]]. Because they both bend in the same way, the ratio of their elastic energies is given directly by the ratio of their flexural rigidities (each proportional to their thickness). The fraction of total energy lost in the coating needs to be multiplied by  $\phi_D$  (of the coating material), and hence Eq. (110). As the oscillation of a thicker object is considered, as long as the coating only bends up and down (e.g., in a drum mode), then we expect the coating contribution to the loss angle to still be proportional to  $\phi_D$ .

As it turns out, the part of coating thermal noise due to bending of the coating-substrate interface [ $S_{z_s z_s}$  in Eq. (87b)] also depends directly on  $\phi_D$ , because the loss mechanism in this case is the same as during the oscillation of a drum mode — one only applies a perpendicular force from below the coating layer, while keeping  $T_{zz} = 0$  within the layer.

It proves less straightforward to connect the thickness fluctuation part of thermal noise [ $S_{u_z u_z}$  in Eq. (87a)] to the effective loss angle of either  $Y$  or  $D$ . Although the loss mechanism here is due to the compressing of a thin membrane from both sides — this membrane is not characterized by vanishing  $T_{xx}$  and  $T_{yy}$ , because the coating is attached to a substrate which provides restoring forces along the transverse ( $x$  and  $y$ ) directions. However, in the case when the Poisson ratio  $\sigma_c$  of the coating vanishes, the thickness fluctuation does depend on the loss angle of the Young's modulus.

For our baseline parameters, mechanical dissipation is mostly contributed by the tantala layers, and because the Young's modulus of the tantala coating material is assumed to be much greater than that of the substrate, the largest contribution to the LIGO mirrors' Brownian noise is bending noise  $S_{z_s z_s}$ . This explains why the noise only varies by 30% (as noted in Sec. VIA) even if no further measurements on the other loss angle is made.

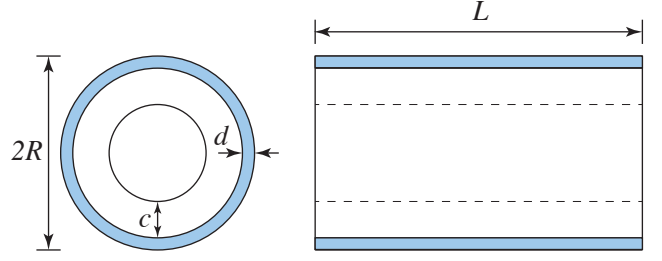


Figure 15: Thin cylindrical shell with thin coating outside. The first torsional eigenmodes of such a shell can be used to measure the shear loss angle of the coating.

### B. Torsional Modes of a Coated Hollow Cylinder

Here we propose an approach with which we can measure another combination of loss angles. We consider a cylindrical shell with a thin, uniform coating layer outside, as shown in Fig. 15 ( $c \ll R$ ,  $d \ll c$ ). In this configuration, the surface deformations produce strains in the plane of shell according to the Donnell shell theory [35]. Here we assumed that there is only angular displacement in the shell, which means the longitudinal position of the cross section won't change. For a torsion mode, we only have shear strain energy, the expressions are given by

$$\frac{U_B}{U} = 0 \quad (111)$$

$$\frac{U_S}{U} = \frac{d Y_c (1 + \sigma_s)}{c Y_s (1 + \sigma_c)}. \quad (112)$$

As a consequence, the total loss angle can be expressed as

$$\phi = \phi_{\text{sub}} + \frac{d Y_c (1 + \sigma_s)}{c Y_s (1 + \sigma_c)} \phi_S \quad (113)$$

For a cylinder shell, according to the Donnell shell theory, the natural frequency of the  $n$ -th torsional mode is given by [36]

$$f_n = \frac{n}{2^{\frac{3}{2}} L} \left[ \frac{Y}{\rho(1 + \sigma)} \right]^{1/2} \quad (114)$$

A more accurate calculation may be found by using the Flügge shell theory [37].

Using the values from Table IV, we can estimate the resonant frequency to be 9.2 kHz. The coating contribution to loss angle, assuming a  $\phi_S$  of at least  $10^{-5}$ , would be at least the order of  $10^{-6}$ , which seems plausible to be extracted from ring-down measurements.

Table IV: Example parameters of a thin, uniformly coated cylindrical shell ( $\text{SiO}_2$ )

	$L$	$R$	$c$	$d$
unit(mm)	200	50	1	0.04

With the measurement of both the thin plate and cylinder shell, we can obtain  $\phi_B$  and  $\phi_S$  of the coating.

material parameter	range	uncertainty in $\sqrt{S_x}$	for details, see
$\phi_B/\phi_S$	0.2 – 5 <sup>a</sup>	±37%	Sec. VIA, Figs. 8, 9.
$Y_{Ta}$	factor of ~ 2	~60%	Sec. VIB, Fig. 10.
$\sigma_{Ta}$	± 0.2	up to 10% if $\phi_B/\phi_S \neq 1$	Sec. VIB, Fig. 11.
$\beta$	-1 < $\beta$ < +1	±1% <sup>b</sup>	Sec. VIC, Fig. 12.

<sup>a</sup>Fixing the combination  $\phi_D$

<sup>b</sup>Calculated from Ta<sub>2</sub>O<sub>5</sub> layers

Table V: Levels of thermal noise uncertainty caused by parameter uncertainties.

## VIII. CONCLUSIONS

In this paper, we applied the Fluctuation-Dissipation Theorem to obtain a *full set of correlation functions* (87a)–(87c) of Brownian thermal fluctuations of a multi-layer dielectric coating. In particular, we have related fluctuations of the coating thickness and the coating-substrate interface to *independent* bulk and shear thermal stresses associated with each coating layer. While those stresses not only induce thickness fluctuations of the layers themselves, they bend the coating-substrate interface and this bending noise had not been previously appreciated intuitively, although its effect has been incorporated into formulas, e.g., in Ref. [14]. As a result, we found that although thickness fluctuations of different coating layers are independent of each other, they each have partial correlations with the height fluctuations of the coating-substrate interface. Moreover, bulk loss creates a positive correlation between them, while shear loss creates a negative correlation. The entire picture is succinctly written mathematically in Eqs. (89) and (90). This coherence structure then gives coating Brownian noise in Eq. (93). Apart from having provided a pedagogical and systematic derivation of these noise components, the most important conceptual consequence of our work is to point out an uncertainty in coating loss angles. We have also incorporated the photo elastic effect, the reflectivity fluctuations of the interfaces within the multilayer coating, and considered the effect of amplitude modulations caused by Brownian thermal noise. All of these turned out to be rather unimportant.

We have applied our formalism to mirrors that are to be used in Advanced LIGO detectors. As estimated in Sec. VI and summarized in Table V (calculated for a typical candidate for the Advanced LIGO end test-mass mirror coating configuration), parameter uncertainties could lead to non-negligible corrections to coating Brownian noise calculations. The biggest uncertainties actually arise from the elastic moduli of coating materials — for example, current uncertainties in Young’s modulus of the tantala coating material might lead up to 60% increase in thermal noise. Although photo elastic coefficients for our coating materials are very uncertain, they do not significantly affect thermal noise since light does not penetrate through many layers.

It is rather remarkable that our lack of experimental knowledge about the loss angles, beyond what we had already ob-

tained from the ring down of drum modes, would not give rise to a higher uncertainty in thermal noise. This is rather serendipitous, considering our path of understanding of the problem: for the baseline parameters of Advanced LIGO, the highest contribution to coating Brownian noise arises from the coating-substrate bending noise caused by losses in tantala layers, because these layers are much more lossy than the silica layers, and have been assumed to have a much higher Young’s modulus than the substrate material. This bending noise, first elaborated by this work, turns out to be associated with the loss angle of the 2-D flexural rigidity, which in turn is directly connected to the decay of the drum modes of a thinly coated sample. This means the currently existing program [14] has been measuring the predominant loss angle all along, and has been compatible with direct measurements of coating thermal noise [15]. Nevertheless, the level of uncertainty noted in our study still warrants further experiments seeking the other loss angle, e.g., as outlined in Sec. VII. In addition, since future gravitational-wave detectors may use different substrate and coating materials, situations may arise when the loss angle measured now does not correlate with the total coating brownian noise.

At this moment, it is worth looking once more at the previously used loss angles,  $\phi_{\parallel}$  and  $\phi_{\perp}$  — although they are mathematically ill defined, they do correctly reflect the existence of two channels of loss. The  $\phi_{\parallel}$  was meant to characterize losses incurred by the  $x$ - $y$  deformations of the coating measurable when we do not compress the coating but instead drive its deformations using drum modes of the substrate. This loss angle is now replaced by the (mathematically well-defined) imaginary part of the flexural rigidity, for which extensive measurements have already been carried out. The  $\phi_{\perp}$  was meant to characterize the losses incurred by compressing the coating layers. This has not been measured because it had not been obvious how to easily excite this mode of coating deformation (the most obvious way would be to compress the coating layer, but that is difficult); however, because the Young’s modulus of the coating is much larger than that of the substrate, this difficult-to-measure loss angle should not contribute as much to the total coating noise. This said, in this work, we do come up with ways to measure both loss angles,  $\phi_S$  and  $\phi_B$ , without having to compress the coating layers — but instead by exciting different modes of substrate deformation. Of course, this is only possible because we have assumed that the material is isotropic — otherwise we may have to compress the coating to directly access the loss induced by such a deformation.

On the other hand, one may think of the possibilities of using substrate materials with higher Young’s modulus to reduce the bending noise. Sapphire and Silicon are two viable choices because they both have higher Young’s modulus than tantala. Using Eq. (87a)–(87c), it is straight forward to estimate the new coating brownian noise while replacing the substrate material by sapphire or silicon but keeping the same aLIGO coating design. It turns out that the coating brownian noise will be reduced to 35% of its original power spectra value if we use silicon substrate or 32% if we use sapphire. However, there are other disadvantages for sapphire or silicon substrate that prevents us from using them for aLIGO mir-

rors. The main problem is that they both have very high thermal conductivity - much higher than fused silica. As a result, the substrate thermoelastic noise is one of the important noise source for both materials. For instance, if the aLIGO mirror was made of sapphire, the bulk thermoelastic noise would have about the same magnitude as the coating brownian noise at 100 Hz. As for silicon substrate, the bulk thermoelastic noise is more than twice larger than its corresponding coating brownian noise because silicon has even higher thermal conductivity than sapphire. One may refer to [40] for detailed methods to calculate bulk thermoelastic noise. Setting up the experiment in a cryogenic environment is a possible way to reduce the thermooptic noise.

Furthermore, our formula Eq. (93) can serve as a starting point for optimizing the material choice and structure design of the multi-layer coating taking light penetration effects into account. Our numerical results in Sec. VID (see Table III) have shown that optimization of the coating structure consistently offers a  $\sim 6\%$  decrease in thermal noise, regardless of  $\phi_B/\phi_S$ . In fact, the optimal structure for these ratios are quite similar, and configurations obtained for each presumed ratio of  $\phi_B/\phi_S$  are shown to work for other ratios interchangeably.

Upon completion of this manuscript, we noted that the optimization of the coating structure for the case assuming  $\phi_B = \phi_S$  (and  $\beta = 0$ ) has been carried out by Kondratiev, Gurkovsky and Gorodetsky [17]. [We note that their formalism is capable to treating  $\beta \neq 0$  and  $\phi_B \neq \phi_S$ , as well as back-scattering induced by photo elasticity, but they did not explore the impact of these effects in their optimization.] Our results are compatible with theirs, if we also use these restrictions in parameter space and ignore back-scattering.

A comparison between our result, Kondratiev et al., and Harry et al. [14] (which ignores light penetration into the layers, and also effectively assumes  $\phi_S = \phi_B$ ) would therefore illustrate the effects caused by ignoring photoelasticity and further ignoring light penetration into the coating. This is shown in Table VI. This again confirms that for total coating thermal noise, light penetration causes noticeable difference in coating thermal noise, while photoelasticity causes a negligible difference.

### Acknowledgments

We would like to thank Stan Whitcomb, Raffaele Flaminio, Jan Harms, Gregg Harry, Yasushi Mino, Valery Mitrofanov, Kentaro Somiya, Sergey Vyatchanin, and other members of the LSC Optics Working Group for very useful discussions. We thank Iain Martin and Andri Gretarsson for many useful suggestions to the manuscript. This work was supported by NSF Grant PHY-0757058, PHY-1068881 and CAREER Grant PHY-0956189, the David and Barbara Groce Startup Fund, and the David and Barbara Research Assistantship at the California Institute of Technology. Funding has also been provided by the Institute for Quantum Information and Matter, an NSF Physics Frontiers Center with support of the Gordon and Betty Moore Foundation.

## Appendix A: Fluctuations of the Complex Reflectivity due to Refractive index fluctuations

Brownian noise is not only caused by random strains, but also by the refractive-index fluctuations induced by such strains, through the photo elastic effect [Cf. Eqs. (13) and (14)]. We will quantify this contribution in this section.

### 1. The photoelastic effect

If we denote the displacement of coating mass elements as  $(u_x, u_y, u_z)$ , then the relative coating-thickness change from its equilibrium value can be written as

$$\delta l/l = u_{z,z} \quad (\text{A1})$$

and the relative transverse area expansion can be written as

$$\delta A/A = u_{x,x} + u_{y,y} \quad (\text{A2})$$

If we denote 2-dimensional displacement vectors along the  $x$ - $y$  plane as  $\vec{u} = (u_x, u_y)$ , and two-dimensional gradient as  $\vec{\nabla}$ , then we have

$$\delta A/A = u_{x,x} + u_{y,y} = \vec{\nabla} \cdot \vec{u} \quad (\text{A3})$$

We can then write the change in refractive index as

$$\delta n = \left[ \frac{\partial n}{\partial \log l} \right]_{A_j} \frac{\delta l}{l} + \left[ \frac{\partial n}{\partial \log A} \right]_{l_j} \vec{\nabla} \cdot \vec{u} \quad (\text{A4})$$

where  $\partial n/\partial \log l$  and  $\partial n/\partial \log A$  only depend on material properties. The two terms on the right-hand side of Eq. (A4) represent refractive index change driven by relative length and area changes, respectively. The first term is given by [28]

$$\beta^L = \left[ \frac{\partial n}{\partial \log l} \right]_A = -\frac{1}{2} n^3 C Y \quad (\text{A5})$$

where  $C$  is the photoelastic stress constant,  $Y$  is the Young's modulus. For silica,  $CY \approx 0.27$ , therefore  $\beta_{\text{SiO}_2}^L = -0.41$ . The photoelastic coefficient can also be written as

$$\beta = -\frac{1}{2} n^3 p_{ij} \quad (\text{A6})$$

where  $p_{ij}$  is the photo elastic tensor [39]. Some experiments have been done to measure this coefficient for tantalum [27]. Empirically, the value of  $p_{ij}$  varies from  $-0.15$  to  $0.45$  for  $\text{Ta}_2\text{O}_5$  thin film fabricated in different ways. Here for the longitudinal photoelasticity,  $\beta_{\text{Ta}_2\text{O}_5}^L$ , we use  $-0.5$  in our numerical calculation.

We shall next obtain formulas that will allow us to convert fluctuations in  $n$  into fluctuations in the complex reflectivity of the multi-layer coating.

Coating	Ref. [14] (no light penetration)	Ref. [17] ( $\beta = 0$ and no back scattering)	This Work
$\lambda/4$	7.18	7.08	7.08
Advanced LIGO	6.93	6.82	6.83
optimal	6.73	6.62	6.64

Table VI: Comparison of thermal noise spectral density (assuming  $\phi_B = \phi_S$  and evaluated at 200 Hz, in units of  $10^{-21} \text{m}/\sqrt{\text{Hz}}$ ) between different works.

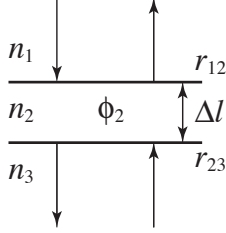


Figure 16: Light propagation across a thin layer (thickness of  $\Delta l$ ) with fluctuating refractive index (from a uniform  $n_2$  to an average of  $n_2 + \delta n_2$  within this thin layer). The propagation matrix corresponding to this structure is given by Eq. (8).

## 2. Fluctuations in an Infinitesimally thin layer

Because the coating is very thin compared with the Rayleigh associated with beam spot size, we model the phase shift of light gained during propagation along  $z$  as only determined the local refractive index. If the refractive index  $\delta n$  at a particular location  $\delta n(z)$  is driven by longitudinal strain  $u_{zz}$  at that location, the fact that  $\langle u_{zz}(z')u_{zz}(z'') \rangle \propto \delta(z' - z'')$  causes concern, because this indicates a high *variance* of  $\delta n$  at any given single point  $z$ , with a magnitude which is formally infinity. If we naively considers the reflection of light across any interface within the coating, e.g., at  $z = z_0$ , then the independent and high-magnitude fluctuations of  $n(z_0-)$  and  $n(z_0+)$  would lead to a dramatic fluctuation in the reflectivity

$$r = \frac{n(z_0-) - n(z_0+)}{n(z_0+) + n(z_0-)} \quad (\text{A7})$$

because, naively,  $n(z_0-)$  and  $n(z_0+)$  are uncorrelated and both have a variance of infinity.

However, two effects prevent the above divergence from actually taking place: (i) there is a finite correlation length for strain fluctuations (although not explicitly given in our current analysis) and (ii) propagation of light averages over those fluctuations. The most convenient way to circumvent the above divergence is to always consider light propagation across a finite layer of materials. As shown in Fig. 16, let us consider three regions in the coating, with refractive indices  $n_1$ ,  $n_2$  and  $n_3$  separated by two interfaces, with the length of the  $n_2$  layer given by  $\Delta l$  — and here we only consider fluctuations in  $n_2$ . The entire transfer matrix (from below to above, in Fig. 16) is given by

$$\mathbf{M} = \mathbf{R}_{r_{12}} \mathbf{T}_{\phi_2} \mathbf{R}_{r_{23}} \quad (8)$$

following the same convention as in Sec. II C. Suppose the originally uniform  $n_2$  now fluctuates, and after averaging over this thin layer, gives a mean refractive index of  $n_2 + \delta n_2$ , we use this as the refractive index of the entire layer, and then have

$$\delta \mathbf{M} = \frac{n_2}{\sqrt{n_1 n_3}} \begin{pmatrix} i & -i \\ i & -i \end{pmatrix} \delta n_2 \cdot k_0 \Delta l \quad (9)$$

Note that when  $\Delta l \rightarrow 0$ ,  $\delta n_2 \cdot \Delta l$  has a variance that approaches zero, and therefore  $\delta \mathbf{M}$  is an infinitesimal matrix — and there is no divergence. [Note that when  $\Delta l$  is small enough,  $\delta n_2$  has a variance that is comparable to the total variance of  $n$ , which is finite — therefore  $\delta n_2 \cdot \Delta l \sim \mathcal{O}(\Delta l)$ .]

The physical meaning of Eq. (9) is the following: a random field of refractive index not only gives rise to a random phase shift (diagonal term), but also gives rise to a random reflectivity (non-diagonal term). The latter term is an additional contribution that has been ignored by previous analytical calculations.

## C. The entire coating stack

Now we are ready to consider the entire multi-layer coating. Let us first focus on layer  $j$  of the coating stack, bounded by two interfaces with reflectivities  $r_{j-1}$  and  $r_j$ , respectively. Since the total transfer matrix of the entire stack is written as

$$\mathbf{M} = \cdots \mathbf{T}_{\phi_{j+1}} \mathbf{R}_{r_j} \mathbf{T}_{\phi_j} \mathbf{R}_{r_{j-1}} \cdots, \quad (10)$$

the reflectivity fluctuations with this layer will contribute to the matrix  $\mathbf{T}_{\phi_j}$  above, which in turn will contribute to fluctuations in the entire  $\mathbf{M}$ . Consider  $dz$ -thick sub-layer located at distance  $z'$  from the  $r_j$  boundary (lower boundary in Fig. 1), therefore at coordinate location  $z = z_{j+1} + z'$  and integrate, we have

$$\begin{aligned} \mathbf{T}_{\phi_j} &\rightarrow \mathbf{T}_{\phi_j} + k_0 \int_0^{l_j} \delta n(z_{j+1} + z) \mathbf{T}_{k_0 n_j z} \begin{bmatrix} i & -i \\ i & -i \end{bmatrix} \mathbf{T}_{k_0 n_j (l_j - z)} dz' \\ &= \begin{bmatrix} 1 & \delta \eta_j \\ \delta \eta_j^* & 1 \end{bmatrix} \mathbf{T}_{\phi_j + k_0 \delta \bar{n}_j l_j} \end{aligned} \quad (11)$$

where

$$\delta \bar{n}_j = \frac{1}{l_j} \int_0^{l_j} \delta n_j(z_{j+1} + z) dz \quad (12)$$



and

$$\delta\eta_j = -ik_0 \int \delta n_j(z_{j+1} + z) e^{2ik_0 n_j z} dz \quad (13)$$

Here we have defined

$$z_j \equiv \sum_{n=j}^N l_n. \quad (14)$$

to be the  $z$  coordinate of the top surface of Layer  $j$ .

We need to adapt the new transfer matrix into the old form, but with modified  $\{r_j\}$  and  $\{\phi_j\}$ . From Eq. (11), since  $\delta\eta_j$  is complex, we need to adjust  $\phi_j$ ,  $r_j$ , as well as  $\phi_{j+1}$ :

$$\begin{aligned} & \mathbf{T}_{\phi_{j+1}} \mathbf{R}_{r_j} \mathbf{T}_{\phi_j} \\ \rightarrow & \mathbf{T}_{\phi_{j+1} + \delta\psi_j^+} \mathbf{R}_{r_j + \delta r_j} \mathbf{T}_{\phi_j + k_0 l_j \delta \bar{n}_j + \delta\psi_j^-} \end{aligned} \quad (15)$$

Here we have defined in addition

$$\delta r_j = -r_j^2 k_0 \int_0^{l_j} \delta n_j(z_{j+1} + z) \sin(2k_0 n_j z) dz \quad (16)$$

and

$$\delta\psi_j^\pm = \frac{r_j^2 \pm 1}{2r_j} k_0 \int_0^{l_j} \delta n_j(z_{j+1} + z) \cos(2k_0 n_j z) dz \quad (17)$$

As we consider photoelastic noise of all the layers together,  $\delta r_j$  in Eq. (16) needs to be used for the effective fluctuation in reflectivity of each layer, while

$$\delta\phi_j = k_0 l_j \delta \bar{n}_j + \delta\psi_j^- + \delta\psi_{j-1}^+ \quad (18)$$

should be used as the total fluctuation in the phase shift of each layer.

#### D. Unimportance of transverse fluctuations

Connecting with the photoelastic effect, we have explicitly

$$\delta n_j(z, \vec{x}) = \beta_j^L u_{zz}(z, \vec{x}) + \beta_j^T \vec{\nabla} \cdot \vec{u} \quad (19)$$

Here the vector  $\vec{u}$  is the two-dimensional displacement vector ( $u_x, u_y$ ) and  $\vec{\nabla} \cdot$  is the 2-D divergence along the  $x$ - $y$  plane. For terms that contain the transverse vector  $\vec{u}$ , we note that when a weighted average of  $\xi$  is taken over the mirror surface [see Sec. II D], they yield the following type of contribution

$$\begin{aligned} & \int_M I(\vec{x}) (\vec{\nabla} \cdot \vec{u}) d^2 \vec{x} \\ &= \int_{\partial M} dl (\vec{n} \cdot \vec{u} I) + \int_M \vec{u} \cdot \vec{\nabla} I d^2 \vec{x} \\ &= \int_M \vec{u} \cdot \vec{\nabla} I d^2 \vec{x} \end{aligned} \quad (20)$$

Here  $M$  stands for the 2-d region occupied by the beam, and  $\partial M$  is the boundary on which power vanishes. As a consequence, the first term is zero according to the boundary condition, while the second term gains a factor of  $(l_i/w_0)$  with respect to other types of coating Brownian noise, here  $l_j$  is the thickness of the  $j$ -th layer, and  $w_0$  the beam spot size. Since we always assume coating thickness  $l_i$  to be much smaller than the beam radius  $r_{\text{beam}}$ , we can neglect refractive index fluctuation due to area fluctuation.

## II. ELASTIC DEFORMATIONS IN THE COATING

Throughout this paper, we assume the mirror substrate to be a half infinite space. We establish a Cartesian coordinate system, with  $(x, y)$  directions along the coating-substrate interface, and  $z$  direction orthogonal to the mirror surface (in the elasticity problem, we also ignore mirror curvature). This allows us to calculate elastic deformations in the spatial frequency domain. We will also assume the coating thickness to be much less than the beam spot size.

We denote the displacement along  $x$ ,  $y$  and  $z$  directions as  $u_x$ ,  $u_y$  and  $u_z$ . It is then straightforward to express the  $3 \times 3$  strain tensor  $\mathbf{S}$  in terms of their derivatives, and stress tensor  $\mathbf{T}$  in terms of Hooke's Law:

$$S_{ij} = \frac{1}{2} \left( \frac{\partial u_i}{\partial x_j} + \frac{\partial u_j}{\partial x_i} \right) \quad (1)$$

$$\Theta = S_{ii} \quad (2)$$

$$\Sigma_{ij} = \frac{1}{2} [S_{ij} + S_{ji}] - \frac{1}{3} \delta_{ij} \Theta \quad (3)$$

$$T_{ij} = -K \Theta \delta_{ij} - 2\mu \Sigma_{ij}. \quad (4)$$

Here we have  $x^j = (x, y, z)$ , with Latin indices (like  $i$  and  $j$ ) running from 1 to 3. Within any layer, it is straightforward to write down the most general solution of the elasticity equilibrium equation

$$T_{ij,j} = 0 \quad (5)$$

as

$$\begin{aligned} \tilde{u}_x &= ik_x [(\tilde{\alpha}_+ + \kappa z \tilde{\beta}_+) e^{\kappa z} + (\tilde{\alpha}_- - \kappa z \tilde{\beta}_-) e^{-\kappa z}] \\ &\quad - ik_y [\tilde{\gamma}_+ e^{\kappa z} + \tilde{\gamma}_- e^{-\kappa z}] \end{aligned} \quad (6)$$

$$\begin{aligned} \tilde{u}_y &= ik_y [(\tilde{\alpha}_+ + \kappa z \tilde{\beta}_+) e^{\kappa z} + (\tilde{\alpha}_- - \kappa z \tilde{\beta}_-) e^{-\kappa z}] \\ &\quad + ik_x [\tilde{\gamma}_+ e^{\kappa z} + \tilde{\gamma}_- e^{-\kappa z}] \end{aligned} \quad (7)$$

$$\begin{aligned} \tilde{u}_z &= -\kappa [\tilde{\alpha}_+ + \tilde{\beta}_+ (-3 + 4\sigma + \kappa z)] e^{\kappa z} \\ &\quad + \kappa [\tilde{\alpha}_- + \tilde{\beta}_- (-3 + 4\sigma - \kappa z)] e^{-\kappa z} \end{aligned} \quad (8)$$

where tilde denotes quantities in the  $x$ - $y$  spatial-frequency domain, and  $\kappa = \sqrt{k_x^2 + k_y^2}$ . Namely

$$u_x(x, y, z) = \int \frac{dk_x dk_y}{(2\pi)^2} \tilde{u}(k_x, k_y, z) e^{-i(k_x x + k_y y)} \quad (9)$$

We now consider a single-layer coating on a substrate, with the coating-substrate interface located at  $z = 0$ , and the coating-air interface at  $z = l$ . Suppose there is a force profile  $F(x, y)$  exerted perpendicular to the surface at  $z = d$ ,  $0 < d < l$ , and let us calculate the elastic deformation field caused by  $F$ . The entire system is now divided into three regions, (a):  $d < z < l$ , (b):  $0 < z < d$ , and (s):  $z < 0$ . At the interfaces, we obtain the following 15 boundary conditions,

$$T_{iz}^a = 0, \quad z = l \quad (10)$$

$$T_{xz}^a = T_{xz}^b, \quad T_{yz}^a = T_{yz}^b, \quad T_{zz}^b - T_{zz}^a = F, \quad z = d \quad (11)$$

$$u_j^a = u_j^b, \quad z = d \quad (12)$$

$$T_{iz}^b = 0, \quad u_j^b = u_j^s, \quad z = 0 \quad (13)$$



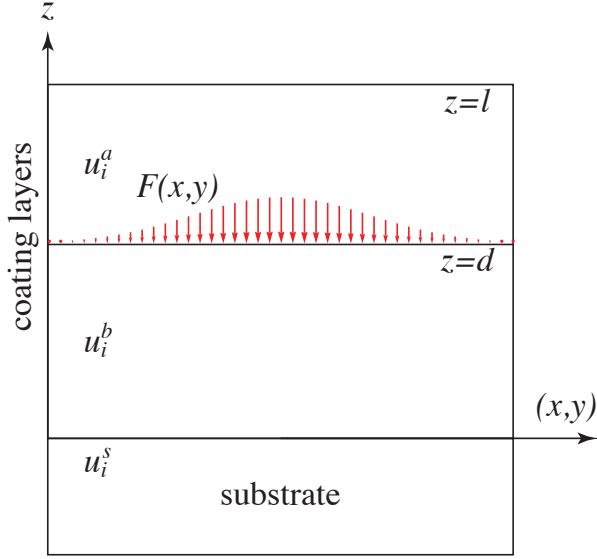


Figure 17: Sample with single layer coating, force is applied perpendicular to the air/coating interface.

as well as the condition that when  $z \rightarrow -\infty$ ,  $u_j^s \rightarrow 0$  (which leads to  $\tilde{\alpha}_-^s = \tilde{\beta}_-^s = \tilde{\gamma}_-^s = 0$ ). We are left with 15 fields

$$(\tilde{\alpha}_\pm^a, \tilde{\beta}_\pm^a, \tilde{\gamma}_\pm^a, \tilde{\alpha}_\pm^b, \tilde{\beta}_\pm^b, \tilde{\gamma}_\pm^b, \tilde{\alpha}_\pm^s, \tilde{\beta}_\pm^s, \tilde{\gamma}_\pm^s) \quad (14)$$

which can be solved from the 15 boundary conditions. Assuming  $\kappa d \ll 1$  and  $\kappa l \ll 1$ , we find that all  $\tilde{\gamma}$  vanish, and

$$\tilde{\alpha}_+^a = \frac{F(1 + \sigma_s)[2 - 3\sigma_s + \sigma_c(-3 + 4\sigma_s)]}{2Y_s\kappa^2(-1 + \sigma_c)} \quad (15)$$

$$\tilde{\alpha}_-^a = \frac{F(\sigma_c - \sigma_s)(1 + \sigma_s)}{2Y_s\kappa^2(-1 + \sigma_c)} \quad (16)$$

$$\tilde{\beta}_+^a = -\frac{F(1 + \sigma_s)(-3 + 4\sigma_s)}{4Y_s\kappa^2(-1 + \sigma_c)} \quad (17)$$

$$\tilde{\beta}_-^a = \frac{F(1 + \sigma_s)}{4Y_s\kappa^2(1 - \sigma_c)} \quad (18)$$

$$\tilde{\alpha}_+^b = \frac{F(1 + \sigma_s)[2 - 3\sigma_s + \sigma_c(-3 + 4\sigma_s)]}{2Y_s\kappa^2(-1 + \sigma_c)} \quad (19)$$

$$\tilde{\alpha}_-^b = \frac{F(\sigma_c - \sigma_s)(1 + \sigma_s)}{2Y_s\kappa^2(-1 + \sigma_c)} \quad (20)$$

$$\tilde{\beta}_+^b = \frac{F[Y_s(1 + \sigma) - Y_c(-3 + \sigma_s + 4\sigma_s^2)]}{4YY_s\kappa^2(-1 + \sigma_c)} \quad (21)$$

$$\tilde{\beta}_-^b = \frac{F[Y_s(1 + \sigma_c) - Y_c(1 + \sigma_s)]}{4YY_s\kappa^2(-1 + \sigma_c)} \quad (22)$$

$$\tilde{\alpha}_+^s = \frac{F(1 + \sigma_s)(-1 + 2\sigma_s)}{Y_s\kappa^2} \quad (23)$$

$$\tilde{\beta}_+^s = -\frac{F(1 + \sigma_s)}{Y_s\kappa^2} \quad (24)$$

We can therefore obtain the strain tensor in the frequency domain for the coating. The non-zero elements for region (a) are

given by

$$S_{xx}^a = \frac{Fk_x^2(-1 + 2\sigma_s)(1 + \sigma_s^2)}{Y_s\kappa^2} \quad (25)$$

$$S_{yy}^a = \frac{Fk_y^2(-1 + 2\sigma_s)(1 + \sigma_s^2)}{Y_s\kappa^2} \quad (26)$$

$$S_{xy}^a = S_{yx}^a = \frac{Fk_xk_y(-1 + 2\sigma_s)(1 + \sigma_s^2)}{Y_s\kappa^2} \quad (27)$$

$$S_{zz}^a = F \frac{\sigma_c(-1 + \sigma_s + 2\sigma_s^2)}{Y_s(-1 + \sigma_c)} \quad (28)$$

while those in region (b) are given by

$$S_{xx}^b = \frac{Fk_x^2(-1 + 2\sigma_s)(1 + \sigma_s^2)}{Y_s\kappa^2} \quad (29)$$

$$S_{yy}^b = \frac{Fk_y^2(-1 + 2\sigma_s)(1 + \sigma_s^2)}{Y_s\kappa^2} \quad (30)$$

$$S_{xy}^b = S_{yx}^b = \frac{Fk_xk_y(-1 + 2\sigma_s)(1 + \sigma_s^2)}{Y_s\kappa^2} \quad (31)$$

$$S_{zz}^b = F \left[ \frac{-(1 + 2\sigma_c)}{Y_c} - \frac{\sigma_c(-1 + \sigma_s + 2\sigma_s^2)}{Y_s(1 - \sigma_c)} \right] \quad (32)$$

Using linear superposition, as well as taking the appropriate limits of the above solution, it is straightforward to obtain elastic deformations in all the scenarios in Sec. IV, with forces applied on various surfaces, that are used to obtain cross spectra between different noises.

### III. DEFINITION OF LOSS ANGLE

In the past [14], the coating loss angle was defined in association with the parallel and perpendicular coating strains. The equation is written as

$$\phi_{\text{coated}} = \phi_{\text{sub}} + \frac{\delta U_{\parallel} d}{U} \phi_{\parallel} + \frac{\delta U_{\perp} d}{U} \phi_{\perp} \quad (1)$$

where  $\delta U_{\parallel}$  and  $\delta U_{\perp}$  are the energy density in parallel and perpendicular coating strains

$$\delta U_{\parallel} = \int_s \frac{1}{2} (S_{xx}T_{xx} + S_{yy}T_{yy}) dx dy \quad (2)$$

$$\delta U_{\perp} = \int_s \frac{1}{2} S_{zz}T_{zz} dx dy \quad (3)$$

and where  $S_{ij}$  are the strains and  $T_{ij}$  are the stresses. While such a definition seems to be compatible with the symmetry of the system, the quantities  $\delta U_{\parallel}$  and  $\delta U_{\perp}$  cannot be used as energy, since in certain scenarios they each can become negative.

For example, if we have a cube with surface area of each side  $A$  (poisson ratio  $\sigma$ , Young's modulus  $Y$ ), and we uniformly apply two pairs of forces, one pair with magnitude  $f$  on opposite  $yz$  planes, the other with magnitude  $F$  on opposite  $xy$  planes, with  $f \ll F$ , as shown in Figure 18. According to

the definition of Young's modulus and Poisson's ratio, up to leading order in  $f/F$  the non-vanishing strains are,

$$S_{zz} = -\frac{F/A}{Y}, \quad S_{xx} = S_{yy} = \sigma \frac{F/A}{Y} \quad (4)$$

On the other hand, for stress, we have, up to leading order in  $f/F$ ,

$$T_{xx} = -f/A, \quad T_{yy} = 0, \quad T_{zz} = -F/A. \quad (5)$$

As a consequence, we have

$$\delta U_{\parallel} = S_{xx}T_{xx} + S_{yy}T_{yy} = -\sigma fF/(A^2Y) < 0 \quad (6)$$

which means  $\delta U_{\parallel}$  is not a reasonable candidate for energy, at least with  $\sigma \neq 0$ . Since it is also true that  $S_{xx}T_{xx} < 0$  we will arrive at

$$\delta U_{\perp} = S_{zz}T_{zz} < 0 \quad (7)$$

if we take this configuration and rotate by 90 degrees around the  $y$  axis, such that  $x$  rotates into  $z$ .

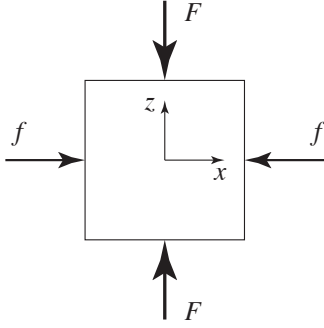


Figure 18: Solid cube with two pairs of forces applied on the side:  $f \ll F$ .

One reasonable way of defining the loss angle is to derive it from the fundamental elastic energy equation. The general form of the stored elastic energy density  $U$  can be written as

$$U = \frac{1}{2}K\Theta^2 + \mu\Sigma_{ij}\Sigma_{ij} \quad (8)$$

$$U_B = \frac{1}{2}K\Theta^2 \quad (9)$$

$$U_S = \mu\Sigma_{ij}\Sigma_{ij} \quad (10)$$

Where  $K$  is called the *bulk modulus* and  $\mu$  is the *shear modulus*. In the calculation, we use Young's modulus  $Y$  and Poisson's ratio  $\sigma$  instead of  $K$  and  $\mu$ . Their relation are given in Eq. (51). The expansion  $\Theta$  and shear  $\Sigma$  are both irreducible tensorial parts of the strain tensor  $S$ .

$$\Theta = S_{ii} \quad (11)$$

$$\Sigma = \frac{1}{2}(S_{ij} + S_{ji}) - \frac{1}{3}\delta_{ij}S_{kk} \quad (12)$$

Note that the expansion and shear energy  $U_B$  and  $U_S$  are always positive, so it is consistent to define the loss angles  $\phi_B$  and  $\phi_S$ .

$j$	$l_j$				
1-5	0.497325	0.208175	0.289623	0.237274	0.250176
6-10	0.245330	0.249806	0.240129	0.270968	0.224129
11-15	0.251081	0.259888	0.260826	0.213460	0.290468
16-20	0.214524	0.273240	0.230905	0.259924	0.230020
21-25	0.275429	0.233086	0.270385	0.208581	0.273798
26-30	0.249741	0.267864	0.204698	0.292317	0.209712
31-35	0.278560	0.220264	0.282694	0.221687	0.268559
36-38	0.233460	0.270419	0.223050		

Table VII: Structure of an Advanced LIGO-like coating optimized jointly for dichroic operation and thermal noise. Thickness of each layer is given in units of wavelength (for light with vacuum-wavelength of 1064 nm) are listed here for the 38 layers. Note that  $l_{1,3,5,\dots}$  are  $\text{SiO}_2$  layers, while  $l_{2,4,6,\dots}$  are  $\text{Ta}_2\text{O}_5$  layers.

#### IV. ADVANCED LIGO STYLE COATING

In Table VII, we provide the structure of the coating optimized jointly for dichroic operation and thermal noise.

- [1] D. Meiser, *et. al.* Phys. Rev. Lett. **102**, 163601 (2009).  
 [2] LIGO Scientific Collaboration, Rep. Prog. Phys. **72** (2009).  
 [3] G. M. Harry (for the LIGO Scientific Collaboration), Class. Quantum Grav. **27**, 084006 (2010).  
 [4] B. Willke *et al.*, Class. Quantum Grav. **23** S207 (2006).  
 [5] The Virgo Collaboration, *Advanced Virgo Baseline Design*, note VIR027A09, May 16, (2009).  
 [6] K. Kuroda (on behalf of the LCGT Collaboration), Class. Quan-

- tum Grav. **27**, 084004 (2010).  
 [7] E. D'Ambrosio, Phys. Rev. D **67**, 102004 (2003); M. Bondarescu and K.S. Thorne, Phys. Rev. D **74** 082003 (2006); M. Bondarescu, O. Kogan and Y. Chen, Phys. Rev. D **78** 082002 (2008).  
 [8] G. Lovelace, Class. Quantum Grav. **24** 4491 (2007); J.-Y. Vinet, Living Rev. Relativity **12** 5 (2009).  
 [9] H. J. Kimble, B. L. Lev and J. Ye, Phys. Rev. Lett. **101**, 260602

- (2008).
- [10] M. Evans *et al.*, Phys. Rev. D **78**, 102003 (2008).
- [11] G. González and P. Saulson, J. Acoust. Soc. Am. **96**, 207 (1994).
- [12] Y. Levin, Phys. Rev. D **57**, 659 (1998).
- [13] H. B. Callen and T. A. Welton, Phys. Rev. **83**, 34 (1951).
- [14] G. M. Harry, A. M. Gretarsson, P. R. Saulson, S. E. Kittelberger, S. D. Penn, W. J. Startin, S. Rowan, M. M. Fejer, D. R. M. Crooks, G. Cagnoli, J. Hough and N. Nakagawa, Class. Quantum Grav. **19**, 897 (2002).
- [15] A.E. Villar *et al.*, Phys. Rev. D **81**, 122001 (2010).
- [16] A. Gurkovsky and S. Vyatchanin, Phys. Lett. A **374**, 3267 (2010)
- [17] N. M. Kondratiev, A. G. Gurkovsky, and M. L. Gorodetsky, Phys. Rev. D **84**, 022001, (2011)
- [18] L. D. Landau and E. M. Lifshitz, *Theory of Elasticity (Course of Theoretical Physics)*, Pergamon (1981).
- [19] I.W. Martin, Class. Quantum Grav. **27**, 225020 (2010)
- [20] G.M. Harry *et al.*, Class. Quantum Grav. **24**, 405, (2007).
- [21] S.D. Penn *et al.*, Class. Quantum Grav. **20** 2917, (2003).
- [22] R. Waynant and M. Ediger, *Electro-Optics Handbook*, McGraw-Hill (1994)
- [23] M. M. Fejer, S. Rowan, G. Cagnoli, D. R. M. Crooks, A. Gretarsson, G. M. Harry, J. Hough, S. D. Penn, P. H. Sneddon and S. P. Vyatchanin, Phys. Rev. D **70**, 082003 (2004).
- [24] P. J. Martin, A. Bendavid, M. Swain, R. P. Netterfield, T. J. Kinder, W. G. Sainty, D. Drage and L. Wielunski, Thin Solid Films **239**, 181 (1994).
- [25] G. M. Harry, M. R. Abernathy, A. E. Becerra-Toledo, H. Armandula, E. Black, K. Dooley, M. Eichenfield, C. Nwabugwu, A. Villar, D. R. M. Crooks, G. Cagnoli, J. Hough, C. R. How, I. MacLaren, P. Murray, S. Reid, S. Rowan, P. H. Sneddon, M. M. Fejer, R. Route, S. D. Penn, P. Ganau, J. M. Mackowski, C. Michel, L. Pinard and A. Remillieux, Class. Quantum Grav. **24**, 405 (2007).
- [26] S. D. Penn, P. H. Sneddon, H. Armandula, J. C. Betzwieser, G. Cagnoli, J. Camp, D. R. M. Crooks, M. M. Fejer, A. M. Gretarsson, G. M. Harry, J. Hough, S. E. Kittelberger, M. J. Mortonson, R. Route, S. Rowan and C. C. Vassiliou, Class. Quantum Grav. **20**, 2917 (2003).
- [27] Y. Nakagawa *et al.*, Electronics and Communications in Japan, **(84)**, 46 (2001).
- [28] J. Stone, Journal of Lightwave Technology **6**, 1245 (1988).
- [29] G. Billingsley, private communication.
- [30] J. Agresti, G. Castaldi, R. DeSalvo, V. Galdi, V. Pierro, and I. M. Pinto, LIGO-P060027-00-Z.
- [31] J. A. Nelder and R. J. Mead, The Computer Journal, **7**, (1965).
- [32] W. H. Press, S. A. Teukolsky, W. T. Vetterling, B. P. Flannery, "Numerical Recipes: The Art of Scientific Computing" (Third Edition), Section 10.5, Cambridge University Press (2007).
- [33] A. Heptonstall, G. Cagnoli, J. Hough, S. Rowan, Phys. Lett. A **354**, 353, (2006).
- [34] S. D. Penn, A. Ageev, D. Busby, G. M. Harry, A. M. Gretarsson, K. Numata, P. Willems, Phys. Lett. A **352**, 3, (2006).
- [35] L. H. Donnell, NACA Report No. 479, (1933).
- [36] Robert D. Blevins, *Formulas for Natural Frequency and Mode Shape*, Van Nostrand Reinhold Company, New York (1979).
- [37] W. Flügge, *Stresses in Shells*, Springer-Verlag, New York (1973)
- [38] S. E. Whitcomb, private communication.
- [39] D. F. Nelson and M. Lax, Phys. Rev. Lett. **24** (1970).
- [40] V. B. Braginsky, M. L. Gorodetsky, and S. P. Vyatchanin, Phys. Lett. A **271**, 303, (2000).